Lawrence Berkeley National Laboratory
Recent Work

Title
X-Ray-Induced Photoelectron and Auger Spectroscopy

Permalink
https://escholarship.org/uc/item/9jp7g0qq

Authors
Perry, Dale L.
Taylor, J.A.
Wagner, C.D.

Publication Date
1990

eScholarship.org Powered by the California Digital Library
University of California

LBL-31267

Lawrence Berkeley Laboratory
UNIVERSITY OF CALIFORNIA

EARTH SCIENCES DIVISION

Published as a chapter in *Instrumental Surface Analysis of Geologic Materials*, D.L. Perry, Ed., VCH Publishers, Inc., September 1990

X-Ray-Induced Photoelectron and Auger Spectroscopy

D.L. Perry, J.A. Taylor, and C.D. Wagner

September 1990

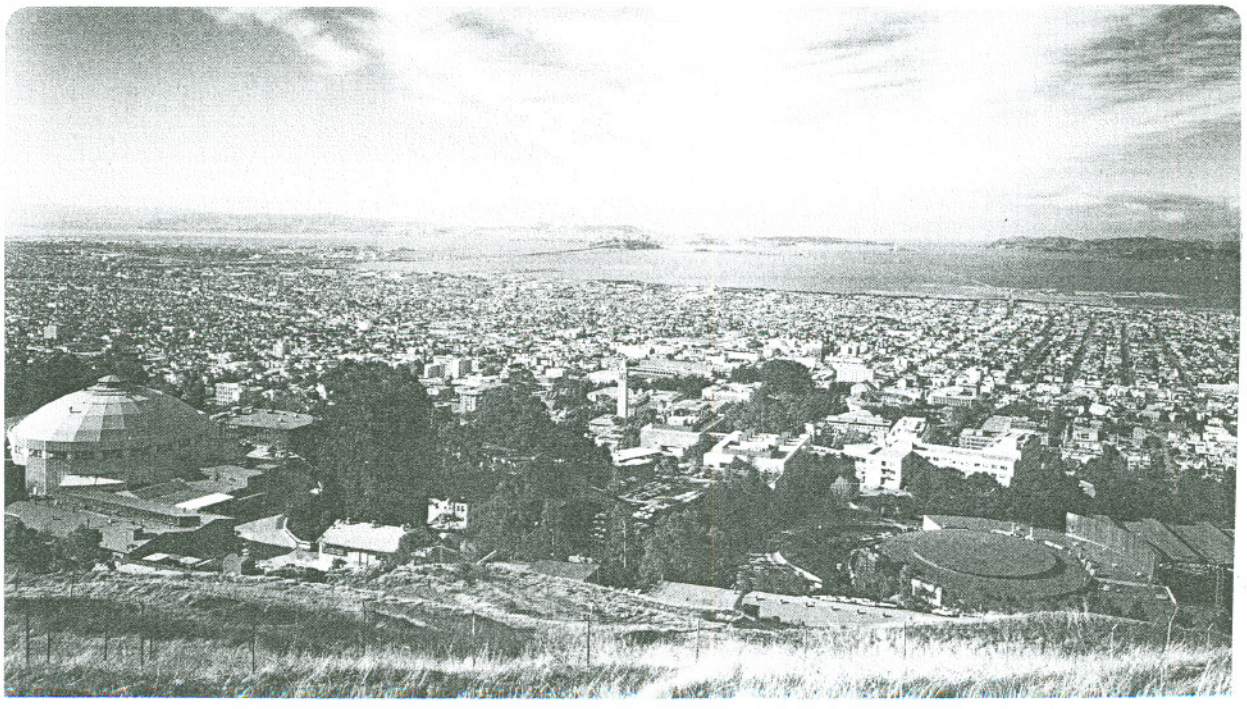

| LOAN COPY |
|Circulates |
|for 4 weeks| Bldg. 50 Library.
Copy 2

LBL-31267

Prepared for the U.S. Department of Energy under Contract Number DE-AC03-76SF00098

DISCLAIMER

This document was prepared as an account of work sponsored by the United States Government. Neither the United States Government nor any agency thereof, nor The Regents of the University of California, nor any of their employees, makes any warranty, express or implied, or assumes any legal liability or responsibility for the accuracy, completeness, or usefulness of any information, apparatus, product, or process disclosed, or represents that its use would not infringe privately owned rights. Reference herein to any specific commercial product, process, or service by its trade name, trademark, manufacturer, or otherwise, does not necessarily constitute or imply its endorsement, recommendation, or favoring by the United States Government or any agency thereof, or The Regents of the University of California. The views and opinions of authors expressed herein do not necessarily state or reflect those of the United States Government or any agency thereof or The Regents of the University of California and shall not be used for advertising or product endorsement purposes.

Lawrence Berkeley Laboratory is an equal opportunity employer.

LBL-31267

X-Ray-Induced Photoelectron and Auger Spectroscopy

Dale L. Perry

Earth Sciences Division
Lawrence Berkeley Laboratory
University of California
Berkeley, California 94720

J. Ashley Taylor

AT & T Bell Laboratories
Allentown, Pennsylvania 18103

Charles D. Wagner

Surfex Company
Oakland, California 94618

September 1990

Published in *Instrumental Surface Analysis of Geologic Materials*
Edited by Dale L. Perry, VCH Publishers, Inc., New York, 1990.

This work was supported by the Director, Office of Energy Research, Office of Basic Energy Sciences, Division of Engineering and Geosciences, of the U.S. Department of Energy under Contract No. DE-AC03-76SF00098.

1. X-RAY-INDUCED PHOTOELECTRON AND AUGER SPECTROSCOPY

Dale L. Perry
Lawrence Berkeley Laboratory
University of California
Berkeley, California 94720

J. Ashley Taylor
AT & T Bell Laboratories
Allentown, Pennsylvania 18103

Charles D. Wagner
Surfex Company
Oakland, California 94618

1. Introduction

X-ray photoelectron spectroscopy (XPS, also known by the acronym ESCA (electron spectroscopy for chemical analysis)) is perhaps the most widely known of the modern ultrahigh vacuum-related surface techniques. Stemming from work reported by Einstein [1] in 1905, the technique takes advantage of the concept that electrons emitted from surfaces being irradiated with soft x-rays can have different kinetic energies as a function of the chemical state of the atom from which they are emitted. The researcher can thus address a wide variety of chemical topics concerning the surface of a geologic material that has undergone a chemical reaction. Information related to surface species and reactions, ie, oxidation-reduction reactions, chemisorption, hydrolysis, and surface dissolution, can be obtained in considerable detail. The paramount advantage of x-ray photoelectron spectroscopy (along with the other experimental techniques in this book) is the ability to gather such surface information as it relates to geologic material interface reactions with gases, liquids, and the products that are formed.

Auger spectroscopy also has its theoretical and experimental roots in the first part of the twentieth century. In 1923, Pierre Auger, while conducting experimental research on the photoelectric effect, reported the existence of the secondary, or Auger, electron in conjunction with the photoelectron while irradiating noble gases with x-rays [2]. The first published account of electron-induced Auger spectroscopy was that of Lander in 1953 [3], and it is by this experimental approach that the bulk of Auger spectra using modern instruments has been obtained.

Several decades elapsed between the experimental proof-of-concept and the development of readily available, commercial instrumentation for performing

research in x-ray photoelectron and Auger spectroscopy. Siegbahn and his co-workers [4] initiated research in the 1950's that addressed the development of high resolution spectrometers that made possible the high precision measurements of kinetic energies of electrons emitted from surfaces. The early research by this group focused on bonding in solids making use of the rather wide range of binding energies of the core electrons. Although the original instrumentation effectively sampled a rather large area of the surface of a material (several square millimeters), newer, more recent instruments have the capability of performing ''small spot'' (approaching several square microns) surface analyses.

While the original Auger research was performed using x-rays to obtain spectra, the technique did not come into its own as a powerful surface analytical technique until the 1960's. The use of electron-induced Auger spectroscopy for surface studies involving deposited cathode-evaporated carbon was reported by Harris [5]. In 1968 Weber and Peria [6] introduced the use of low-energy electron diffraction instruments as an approach for recording Auger spectra. Finally, Palmberg et al [7] introduced the use of the cylindrical mirror analyzer to obtain the rapid acquisition of Auger spectra coupled with high sensitivity. More recent studies of x-ray-induced Auger spectra (observed during the recording of x-ray photoelectron spectra of samples) have shown that much information can be obtained from surfaces using this combined approach. Advances continue to be made in instrumentation in both x-ray photoelectron and Auger spectroscopy, while the growth in applications of the techniques appears to continue unabated. This is especially true in the areas of analytical and surface chemistry of geologic materials.

The present work is written to provide an introduction to combined x-ray photoelectron and Auger spectroscopy as it relates to geologic materials. In

addition to the basic principles of the two techniques, numerous applications involving surface chemical reactions and surface morphology changes are discussed. Interface reactions involving such geologic species as silicates, aluminosilicates, and sulfides are subjects of several previous studies; these materials have been studied from both basic natural alteration (or weathering) processes of the materials under geologic conditions and the addition of chemical species through gaseous or liquid phases. The result of this treatise should be a better understanding by the reader of existing applications of the techniques and an awareness of new applications of which they have not been previously aware. However, it is important that the reader should consult more detailed and extensive treatises on x-ray photoelectron [8-15] and Auger [12-16] spectroscopy. He should also refer to various annual reviews that compile the most recent advances in both fields; one of the best ongoing series of annual reviews is that found in *Analytical Chemistry* [17–31].

2. *X–Ray Photoelectron and Auger Spectroscopy*

2.1. Basic Principles. The principles of conducting the x-ray photoelectron experiment are quite straightforward. A source of soft x-rays (usually either Mg Kα or Al Kα at 1253.6 and 1486.6 eV, respectively) is directed onto the surface of a sample housed in a vacuum chamber of an x-ray photoelectron spectrometer, with the pressure in the chamber being typically in the range of $10^{-8} - 10^{-11}$ torr. The ensuing ejected photoelectron (Fig 1.) is then collected by an analyzer which measures the kinetic energy of that electron. The kinetic energy is translated into a binding energy for the specific atomic orbital of that electron according to Eq. 1

$$E_k = h\nu - E_b - \phi_s \quad (1)$$

where E_k is the kinetic energy of the electron, $h\nu$ is photon energy supplied by the source anode, E_b is the binding energy of the corresponding elemental orbital, and ϕ_s is the work function [32] of the spectrometer. The resulting spectrum mirrors the top 10–50 Å of the surface (the escape depth of the Auger and photoelectrons which comprise the spectrum) appears as a collection of peaks as shown in Figure 2 [33]; the 0–1000 eV range covered is referred to as a ''survey'' spectrum and includes the x-ray photoelectron lines associated with the chemical elements present on the sample surface. The sensitivity for detecting elements lies in the range of 0.1–0.5% atomic concentration for both x-ray photoelectron and Auger spectroscopy. In addition to the *qualitative* chemical information obtained about the chemical surface states, *quantitative* information about the surface can be derived also. This can be achieved, however, only with the use of rigorous, precise standards for comparison, and the best absolute value obtained still has an error of ± 1–5%. Because of sample roughness and differences in thickness of contaminant layers, absolute quantitative measurements (such as those typically made with the electron microprobe) are rarely used. Relative atomic concentrations are made extensively by measuring the line intensities for different atoms and dividing them by generalized sensitivity factors or by a set which the investigator has empirically determined by himself [34,35]. The set of corrected intensities are then normalized to 100%. This gives essentially the atomic ratio of any two elements in the sample. By doing so, the investigator can get a true picture of elemental concentration changes from one reacted surface to another involving the same elements.

In addition to the ejection of the photoelectron shown in Figure 1, there is the emission of the Auger electron. Formed by the relaxation of the energetic ion

left after the emission of the photoelectron, the process involves an outer electron falling into the "hole" created by the lost photoelectron. A secondary, or Auger, electron is then emitted which exhibits a kinetic energy that is the difference between the initial ion and the doubly charged final ion. In general, the Auger lines observed in a combined XPS/Auger spectrum are more electronically (and thus geometrically) complex than the photoelectron lines.

There are four principal series of Auger lines that appear along with x-ray photoelectron spectra, those being the KLL, LMM, MNN, and the NOO lines. The first letter designates the hole level of the ejected photoelectron, while the last two letters designate the level of the double vacancies created by the Auger process. Thus, the Auger process in Figure 1 represents that of the KLL series of the oxygen atom. Table 1 lists a group of both x-ray photoelectron and Auger lines that are available for studies of the major elements in a variety of mineral systems. While not intended to be exhaustive, the list does contain a rather wide array of possible lines for study concerning those minerals.

2.2. Sample Considerations. In addition to the instrumental requirements for performing x-ray photoelectron and Auger experiments, there are also practical considerations as to what samples can be studied. The solid samples must be vacuum-amenable and not be susceptible to decomposition in the $10^{-8} - 10^{-11}$ torr range. The samples can be in the form of both powders and continuous solids such as wafers, chips, and thin films. In the case where an unreacted sample is being used as a standard, it should be as fresh a specimen as possible and free from contamination. Reacted samples which are to be studied should be introduced into the spectrometer without disturbing or altering the reacted surface, since this would produce a spectrum which would not be representative of the true, chemical state in the spectrometer chamber, while powders have to be

mounted on ultrahigh vacuum-amenable tape, pressed between indium foil, or pressed into pellets. All of these techniques have well-documented advantages and disadvantages, and the reader is encouraged to consult standard references which discuss the preparation and manipulation of samples in detail [33].

While this precludes studying samples which are actually wet at room temperature, it does not dictate a *pro forma* exclusion of samples that have been

Table 1. Suitable Lines for Combined X-Ray Photoelectron/Auger Studies of Selected Mineral Systems.

Element	Photoelectron Line	Auger Line	Mineral System
Aluminum[a]	1s	$KL_{23}L_{23}$	Aluminates, aluminosilicates
Silicon[a]	1s	$KL_{23}L_{23}$	Silicates, aluminosilicates
Oxygen[b]	1s	KVV	Oxides
Sulfur[c]	1s	KVV	Sulfides
Iron[b]	$2p_{3/2}$	L_3VV	Iron oxides, hydroxides, sulfides
Selenium[b]	$3d_{5/2}$	$L_3M_{45}M_{45}$	Selenium oxides, and selenium oxyanions
Phosphorus[c]	1s	$KL_{23}L_{23}$	Phosphates

[a] Au Mα (2122.9 eV) source

[b] Al Kα (1486.6 eV) source

[c] Ag Lα (2984.3 eV) source

reacted with solvents such as water. Alterations of a surface that have been in the presence (and thus contains molecules of) of liquid reagents can indeed occur; however, if they are chemically bonded to the surface, their chemical state will be reflected in the spectrum. Indeed, thousands of studies involving normally liquid molecules reacting with solid materials exist in the surface chemistry

literature. The sample can also be studied at a cooled temperature to minimize change in the sample surface. Conversely, however, the investigator must take the same precautions in studying these solvent-reaction systems as he does in studying any other ones. The most effective way of monitoring any surface changes in the course of an experiment is to conduct the experiment *as a function of time*. If the spectra remain unchanged and the samples remain visibly constant (i.e., no discoloration occurs) during the course of experiments on a sample, the sample can be assumed to be stable. This is the same caveat that must be observed for studying all chemical systems by any type of spectroscopy.

There are a number of other well documented problems involving surface alterations during the x-ray photoelectron and Auger experiment in addition to dehydration that can confront the investigator, one of the chief ones being that of charging. This problem can be a pronounced one, especially in cases where the sample being studied is an insulator. Recalling that the basic, initial process involved in the x-ray photoelectron experiment is the ejection of a negatively charged electron, one realizes that this leaves a positively charged sample surface. If the sample is not able to achieve electrical equilibrium by an electron flow from ground or by electron acquisition from the vacuum space, a positive charge accumulates on the surface which cannot be dispersed. This effect manifests itself in both subtle and gross ways. In cases where the charging is rather weak or intermediate, increases in the binding energy and photoelectron linewidth are observed. Severe levels of charging, however, may result in the appearance of multiple photoelectron lines, and many such cases have been reported in the literature. This occurs especially with heterogeneous samples such as conductors embedded in insulators. These effects can be minimized by the use of a flood gun which provides a source of compensating electrons to the

surface [33,36].

There are several methods for treating or correcting peak shifts due to charging. The most common one is the use of the so-called ''adventitious'' carbon 1s line which is introduced to the sample surface both by atmospheric handling and by the spectrometer system itself. This line has been experimentally determined to occur at 284.8 eV, so its shift in a spectrum can be assumed to result from charging. This shift is then used to adjust the binding energy values for the other lines in the spectrum. Other often used techniques include the use of an internal standard element (such as the silicon 2p line in aluminosilicates) for appropriate samples and the use of gold decoration. In the latter technique, a very thin film (or trace) of gold is evaporated onto the sample after it has been studied; the ensuing spectrum is then calibrated against the binding energies of the intense gold $4f_{7/2,5/2}$ lines.

One potentially serious experimental problem for studying some chemical surface systems is that of metal ion reduction. Metal ions which are susceptible to x-ray beam reduction during the course of XPS/Auger studies are ones which are in a rather high oxidation state initially and may form stable, lower oxidation states. Hexavalent uranium, for example, can undergo photoreduction to the uranium(IV) species which in turn can be reduced still further to the metal itself. One of the most thoroughly studied metal ion reduced systems is that of the copper(II) ion. This reaction has been reviewed [37], and it seems to be the most severe for copper(II) oxide and copper(II) halides. Several mechanisms for the reduction of the former compound have been published [38-40].

Another problem sometimes encountered is that of sputter-induced metal ion reduction. In an attempt to clean or depth-profile a surface, an investigator

may use argon ion sputtering, or bombardment, for this purpose. The result may be the reduction of a high oxidation state metal ion to a lower oxidation state. Again, the sputter-reduction of copper(II) has been studied by Yamada et al. [41]. Brundle and his co-workers [42] have demonstrated that both Fe_3O_4 and Fe_2O_3 can be reduced by sputtering. One way of circumventing the problem is to vary the angle between the plane of the sample surface and the analyzer entrance angle [33]. Thus the investigator can obtain a limited depth profile of a material without altering the surface.

By inspection of the survey spectrum shown in Figure 2, one can see that differences exist among the various x-ray photoelectron lines with respect to their intensity and shape. Additionally, the Auger lines are found along with the photoelectron lines, and it is this ability to generate both x-ray photoelectron and Auger data in the same spectrum that makes the Auger parameter discussed below such a useful tool. A detailed, high-resolution study of these lines, along with their associated satellites and fine structure, yields a wealth of information about the chemistry and bonding of geologic surfaces. The following discussion of several of the aspects of the spectral parameters will give a clearer picture of their application in understanding surface properties and surface phenomena.

2.3. Spectral Parameters

2.3.1. Binding Energy and Auger Shifts. The numerical positions of the x-ray photoelectron lines for the different elemental orbitals shown in Figure 2 are referred to as the binding energies; the kinetic energies of the Auger lines (or, more correctly, the collection of lines comprising the Auger peak) are also presented in terms of a binding energy. The binding energy is easily the most widely quoted experimental value in x-ray photoelectron spectroscopy. The core

level binding energies of elements can many times be used to differentiate between several different oxidation (and thus chemical species) states of an element. These binding energy changes as a function of oxidation state can vary by a fraction of an electron volt or several electron volts over the entire range of oxidation states for an element. In the case of tin, for example, there is a binding energy difference of less than two electron volts between zerovalent, elemental tin and the tin(IV) state; for purposes of differentiating between tin(II) and tin(IV), the separation is sometimes almost negligible, depending on the species of the two oxidation states being studied. A broad range of binding energies, however, is exhibited by sulfur, ranging from ≈ 162 eV for the sulfide (S^{II-}) to ≈ 168 eV for the $S^{VI}\,O_4^{-2}$ anion.

Auger shifts, however, will often exceed photoelectron binding energy shifts for elements. One study of Auger and photoelectron lines of the oxides of a series of elements revealed that the shift of the Auger line could be from two to ten times that of the shift of the photoelectron binding energy [43]. Two conditions must be met if this large ratio of Auger shift to photoelectron shift is observed. First, the element is a conductor, and secondly, the initial vacancy in the Auger process must be effected in the inner shell. Several elements such as sodium, cadmium, silver, zinc, magnesium, and copper display quite large Auger shifts compared to their relatively small photoelectron binding energy shifts. More detailed treatises on the relationship between the two parameters can be obtained from the literature [44,45].

2.3.2. Spin-orbit splitting. During the ionization of a p, d, or f orbital in the photoelectron emission process, one of the direct results is the formation of two ionic states. These two states are represented by a so-called spin-orbit doublet in the x-ray photoelectron spectrum. For the p orbital, the two lines are

designated as the $p_{3/2,1/2}$ doublet, for the d lines, $d_{5/2,3/2}$, and for the f lines, $f_{7/2,5/2}$. The two major lines shown in the spectrum in Fig. 3, for example, represent the $2p_{3/2,1/2}$ spin-orbit doublet for chromium(III), with the values for the chromium $2p_{3/2}$ and chromium $2p_{1/2}$ being 577.0 and 586.4 eV, respectively. The spin-orbit splitting is merely the difference between these lines, or 9.4 eV. Many times, the spin-orbit splitting is coupled to the oxidation state of the metal ion and/or the electronic "spin-state" of the ion. This is the case for cobalt, where the spin-orbit splitting difference can be used to differentiate between the paramagnetic "high-spin" cobalt(II) ion and the diamagnetic cobalt(III) "low-spin" species [46]. The reader is referred to other treatises [8,9,47] for a more comprehensive discussion on spin-orbit splitting of elements.

2.3.3. Multiplet Splitting. During the process of emitting a core level photoelectron, such as from the chromium 2p level shown in Figure 3, the phenomenon is not an isolated event. Rather, when the event is coupled by interaction with one or more valence shell electrons, a second phenomenon, that of multiplet splitting, is also observed. The concept of multiplet splitting [48] can be quite useful in studying paramagnetic metal ions, since the electronically unpaired "hole" created in the core level is interacting with unpaired electrons in the valence shell (in the case of chromium, the 3d electrons). The 3d metal ions that are paramagnetic, all of which are members of the first row transition metal ions, exhibit broadening of their 2p photoelectron spectra. While not readily obvious due to overlap of the two doublets, the $2p_{3/2,1/2}$ lines attributable to the chromium(VI) species in Fig. 3 are narrower than the lines attributable to the chromium(III) species. The reason for this is that the chromium(III) compound on the surface is an unpaired $3d^3$ electronic system and is thus exhibiting multiplet splitting; this paramagnetic configuration is in opposition to that of the

chromium(VI) species, a 3d° diamagnetic configuration. A second manifestation of multiplet splitting in paramagnetic 3d ions is an actual splitting of the 3s photoelectron level of the ions. Thus, the investigator can observe both different binding energies and different separations in the doublet peaks in this level [49] for various compounds. This can be used in conjunction with model compounds to identify a particular surface species or, conversely, to rule out a suspected species.

2.3.4. "Shake-up" and "Shake-off" Satellites. Two more types of configurational interactions, similar in nature to that of multiplet splitting, are those of "shake-up" and "shake-off." Under normal conditions, an x-ray photoelectron possesses a relatively large kinetic energy and is most often removed from its core orbital without causing additional excitation of other electrons. Some electronic relaxation always occurs which affects the kinetic energy of the photoelectron, but if additional (often less probable) interactions occur between the photoelectron and the valence electrons during the ionization event, the photoelectron will lose some of its energy, and additional peaks will be observed in the spectrum. These peaks will occur as satellite structure located to the high binding-energy side of the main peak. Two possibilities are often discussed. First, another electron can be promoted to an excited state; this process is called "shake-up". If, however, that electron is promoted to a continuum state, the process is referred to as "shake-off". The various energy-loss processes can be specifically identified for simple gases, but for solids this structure often exists as one or more broad bands.

The position and shape of these satellite structures can often be used as a fingerprint to identify the chemical species on the surface without having to assign the energy-loss mechanism. The most intense satellite structure is

observed for the transition metals [50,51] and rare earth compounds which possess unpaired electrons and are therefore paramagnetic species. Thus, high-spin cobalt(II) (d^7), high-spin iron(III) (d^5), high-spin iron(II) (d^6), nickel(II) (d^8), chromium(III) (d^3), and copper(II) (d^9) complexes give very strong satellites with resolvable fine structures in most cases. In several of these metal ion systems, differentiation between different complexes of the same metal ion can be effected on the basis of the difference in their satellite structure. A good review of the rules describing the variation in the satellite structure as a function of the various electronic types of metal ions and their satellite patterns can be found in the literature [52].

2.3.5. Plasmon Loss Lines. For solids another energy-loss mechanism, the plasmon loss, must also be considered. The observed satellite structure is then a combination of both intrinsic and extrinsic losses. The intrinsic losses would include the ''shake-up'' or any other relaxation mechanism similar to those described in Section 2.3.4. These are associated with the ionization event itself. However, an electron passing through a solid can interact wit the valence or conduction electrons of the solid giving up some of its energy in discrete amounts, ΔE_L. This is then the extrinsic or plasmon loss contribution. The energy-loss shift ΔE_L is measured simply by taking the difference in binding energy between the main photoelectron lines (A1 2s for the example shown in Fig. 4) and the first energy-loss peak. For the plasmon loss, in the simplest model, the photoelectron interacts with the free electron gas in a metal,

$$\Delta E_L = \frac{h}{2\pi} (4\pi e^2 n/m)^{1/2} = \frac{h}{2\pi}\omega_p \qquad (2)$$

where e and m are the charge and mass of the electron, n is the density for the electrons, and h is Planck's constant. The loss is said to be that of a bulk

plasmon if the excitation occurs within the solid. For some metals such as aluminum, a surface plasmon loss [53] equal to $\Delta E_L / \sqrt{2}$ also is observed. The plasmon loss is proportional to the electron density which is specific to each individual metal, so that E_L can be used to identify different metals. It has also been shown that ΔE_L is independent of sample charging, and it has been argued that the plasmon-loss effect is independent of relaxation, or it represents changes in the initial electronic state [69,70]. The intrinsic losses are due to relaxation during the photoionization process and thus represent changes in the final states. Plasmon interactions also occur for wide band-gap materials with the photoelectron interacting with the valance bands if they are highly delocalized and collectively shared. As the band gap increases forming good insulators, it becomes more difficult to separate the intrinsic and extrinsic effects [69]. For many materials, the plasmon losses dominate the spectrum, and this is most likely true for the aluminum and silicon compounds. For compounds of the transition metals, as previously noted, the intrinsic loss can be very strong, obscuring the plasmon losses. The energy-loss shift has been shown to change significantly for many different compounds [69], and if the loss structure is comprised mainly of plasmon losses, changes in ΔE_L will indicate changes in the initial electron densities for the material.

Figure 4 illustrates a good example of using plasmon loss lines to follow the oxidation of a clean aluminum surface to form an overlayer of alumina, Al_2O_3 [55]. In the bottom spectrum, one sees an evaporated film of aluminum metal with no oxidation; the bulk plasmon losses are separated by 15.2 eV, while the surface plasmon losses are separated by 10.7 eV. Upon exposure to oxygen at atmospheric pressure for thirty minutes, however, an overlayer of Al_2O_3 has formed. As would be expected, surface plasmon losses attributed to the elemental, unoxidized aluminum are absent. Completely oxidized aluminum has a ΔE_L

of about 24 eV.

3. *Auger Parameter*

The experimental binding energies are derived from Eq. 1 using the values of hυ, ϕ_s, and the measured kinetic energy E_k. The measured binding energies thus obtained are equal to the difference in total energy of final state ion and the initial state of the compound.

$$E_b = E_f - E_i \tag{3}$$

It is emphasized that the difference in the measured binding energies has both changes in the initial state due to chemical changes and to changes in the final ionized state due to rearrangement of orbitals as a consequence of the ionization process. These two contributions cannot be separated by just measuring shifts in the core binding energies. Often, for similar compounds, the final state changes are similar, and one sees a predicted shift in binding energies with a change in chemistry; however, this is not observed for all compounds.

Another way of defining the binding energy is to set it equal to the orbital energy of an electron occupying the initial or un-ionized energy level minus a relaxation energy, R.

$$E_b(i) = \varepsilon(i) - R \tag{4}$$

The relaxation energy [56] can be loosely divided into two parts: intraatomic and extraatomic. Intraatomic relaxation includes the rearrangement of any orbital due to the ionization event, occurring for any atom, isolated or not, and is invariant to any changes in the environment surrounding the atoms. Extraatomic relaxation arises from the redistribution of electrons in neighboring atoms or in the conduction band of a metal. Extraatomic relaxation is also known as the

polarization energy or screening energy, since the electrons rearrange themselves to screen the hole produced in the core orbital to obtain a minimum energy configuration.

Such a distinction may seem arbitrary, but as will be shown, there is a way to directly measure the extraatomic relaxation. The change in binding energy for various chemical compounds from Eq. 4 for the photoelectrons is

$$\Delta E_b(i) = \Delta\varepsilon(i) - \Delta R^{ea}(i) \tag{5}$$

The relaxation energy now is essentially extraatomic, since the intraatomic part will be about the same for different compounds containing the same atom. For the shift in the Auger line, three energy levels (ijk) must be considered.

$$E_k(ijk) = E_b(i) - E_b(j) - E_b(k) - e(jk) + R(jk) \tag{6}$$

The term e(jk) is the interaction energy of the two holes in the final state. R then is the total relaxation energy with both intra and extraatomic contributions. The change in the Auger kinetic energy from chemical changes would be

$$\Delta E_k(ijk) = \Delta E_b(i) - \Delta E_b(j) - \Delta E_b(k) + \Delta R^{ea}(jk) \tag{7}$$

For KLL Auger transitions, several approximations can be made.

$$\Delta R^{ea}(LL) \approx 2\Delta R^{ea}(K) \tag{8}$$

$$\Delta E_b(K) \approx \Delta E_b(L) \tag{9}$$

Equations 6, 7, and 8 can then be combined to give

$$\Delta E_k(KLL) \approx -\Delta\varepsilon(K) + 3\Delta R^{ea}(K) \tag{10}$$

By comparing Eqs. 5 and 10, one notes that in general the chemical shift for Auger lines will not be the same as for the photoelectron lines because of the sig-

nificant difference in ΔR^{ea} associated with the two-hole Auger final state as compared to ΔR^{ea} for direct photoionization. In fact, the chemical shift for the Auger lines is often much larger.

If both the binding energy of the photoelectron and the kinetic energy of the Auger electron are measured, a new parameter, known as the Auger parameter (α), can be determined. Wagner originally defined the Auger parameter (α_w) [57] as the difference between the kinetic energy of the most intense Auger line ($E_k(ijk)$) and the most intense photoelectron line ($E_k(i)$).

$$\alpha_w = E_k(ijk) - E_k(i) \tag{11}$$

E_k, the kinetic energy, then equals

$$E_k(i) = h\nu - E_b(i) \tag{12}$$

In this case the reference is assumed to be made from the Fermi level rather than the vacuum level (Eq. 1), and $E_k(\text{Fermi}) = E_k(\text{vacuum}) + \phi_s$. The definition of the modified Auger parameter [58], as currently used in most papers, is obtained by combining Eqns. 11 and 12.

$$\alpha = \alpha_w + h\nu = E_k(ijk) + E_b(i) \tag{13}$$

$$\alpha + h\nu = E_k(\text{Auger}) + E_b(\text{photoelectron}) \tag{14}$$

The modified parameter as so defined is then independent of $h\nu$ and is always positive. As shown in Fig. 5, the actual measurement of the Auger parameter is simply the difference in the kinetic energy between two lines. This difference will remain the same independent of sample charging because any charging shifts will cancel. This is important for geologic materials, since many are insulators and thus exhibit charging. For the same reason, the Fermi level does not need to be precisely determined; data referenced to the vacuum level can also be directly

compared. Often binding energy data and Auger kinetic energy data are combined creating a two dimensional plot as shown in Figs. 6 and 7. Of course the binding energy data must be referenced to the Fermi level and corrected for charging. Changes in the binding energies of photoelectron lines are taken from the x-axis, and the changes in the kinetic energies of the Auger lines are determined from the y-axis. As previously described, they are usually not the same. The plot then defines the Auger parameter (Eq. 14) as a series of diagonal lines. Any points lying on the diagonal would represent equal Auger parameters. By constructing such two-dimensional plots, much more chemical information can be extracted from the x-ray photoelectron spectra.

The Auger parameter of many different compounds has been measured and tabulated, showing that the parameter changes with the chemical environment [59,60]. For KLL Auger transitions, Eqns. 5 and 10 can be combined giving

$$\Delta\alpha = 2\Delta R^{ea}(i) \qquad (15)$$

This states that the change in the Auger parameter in the first approximation [61] is a direct measure of the change in the extraatomic relaxation. A fair question to ask is whether the extraatomic relaxation has any physical meaning. A number of studies have indicated that it is directly related to the polarizability of the material. The polarizability arises from various electronic interactions with the hole produced by the ionization, and these interactions slightly affect the kinetic energy of the escaping electron [62]. For good dielectrics a slight displacement of the negatively charged electron cloud of neighboring atoms occurs in response to the production of the positive hole. For ionic crystals, anion and cation interactions dominate [63]. If the material possesses a permanent electric dipole, this would be another source of interaction. For conductors, charge is no longer

bound and thus is free to move within the conduction band to more completely screen the hole.

All of these interactions are of course additive, but often for a specific class of materials, one will dominate [63]. For example consider various sodium compounds [59]. A gaseous sodium atom possesses the smallest Auger parameter because the extraatomic relaxation energy would be zero. Metallic sodium, a good conductor, has the highest Auger parameter, because the polarization energy or extranuclear relaxation term is large. The difference between the Auger parameter of the gaseous atom and any other compound yields its extraatomic relaxation or polarization energy. The Auger parameter for the rest of the sodium ionic salts lie between these values, with NaI greater than most of the salts and NaF less than most of the other salts. Studies have also been conducted on frozen aqueous solutions of various sodium salts [64]. Results showed only small changes in the Auger parameters for all of the sodium salts in solution; a much greater change was observed for the solid ionic salts. For the frozen aqueous solutions, the Na^+ is surrounded by a similar environment of water molecules for each case. In general, the greater the polarizability of the compound, the greater the Auger parameter will be.

The application of the Auger parameter using x-ray induced photoelectron and Auger lines in the same spectrum can be effected by considering what photoelectron and Auger lines are present for the elements of the material to be studied. Figure 5, for example, shows the lines used to obtain the Auger parameter for sodium hydrogen phosphate, Na_2HPO_4. Even in a pure compound, however, this can sometimes be difficult because of the close proximity of some of the lines to one another. In the case of uranium oxides, a detailed study of the uranium $4d_{5/2,3/2}$ photoelectron lines is difficult because of the complex oxygen

KLL Auger peaks which occur in the same region. This also makes the study of related materials such as uranium aluminosilicates and other uranium-oxygen systems quite complex. The same situation exists for chromium and vanadium systems of oxygen where the oxygen KLL Auger peaks overlap the chromium/vanadium LMM peaks. For cases such as these, the investigator must rely not only on the positions of photoelectron and Auger lines but also a quite detailed and careful lineshape analysis of all of the various components.

While these problems do hinder the use of the Auger parameter concept to geologic studies in several cases, there are indeed many applications for which it is a powerful tool. In the following discussion, its use is detailed in the study of such areas as bonding in geologic materials, sorption studies, and surface chemical modifications as they relate to such areas as mineral processing and flotation. Table 2 contains a representative sample of different applications of x-ray photoelectron and combined x-ray photoelectron/Auger spectroscopy to geologic materials, both in their pristine and reacted states. While certainly not intended to be a comprehensive compilation, it presents a fair balance with respect to possible applications.

Table 2. Applications of X-Ray Photoelectron and Combined X-Ray Photoelectron/Auger Techniques to Geologic Studies.

Type of Study	System Studied	Technique(s)	Reference
Structure	Titanates	XPS	[75]
	Aluminosilicates	XPS	[65]
	Aluminosilicates	XPS	[66]
	Aluminosilicates	XPS	[72]
	Aluminosilicates	XPS	[73]
	Silicates	XPS	[74]
	Zeolites	XPS	[67]

Table 2. (Continued)

Type of Study	System Studied	Technique(s)	Reference
	Micas	XPS	[71]
Analysis	Coal macerals	XPS	[76]
	Sediments	XPS	[79]
	Biological minerals	XPS	[12]
	Kerogens, coal	XPS	[77]
	Sediments, soils	XPS/AES	[78]
	Mt. St. Helens ash	XPS	[108]
Electronic state	Hollandites	XPS	[80]
	Forsterite	XPS	[81]
	Manganese oxides	XPS	[82]
	Lepidolite, manganese oxides	XPS	[83]
	Copper minerals	XPS	[84]
	Copper minerals	XPS/AES	[85]
	Copper minerals	XPS	[86]
	Vanadium aegirines	XPS	[87]
	Iron clay minerals	XPS	[88]
	Garnierite	XPS	[89]
	Lead minerals	XPS/AES	[90]
	Carbonate minerals	XPS	[91]
Reaction chemistry	Imines on mica	XPS	[109]
	Metal ions on sulfides	XPS	[93]
	Metal ions on sulfides	XPS/AES	[110]
	Oxidation of sulfides	XPS	[100]
	Organics on pyrite	XPS	[102]
	Reactions of asbestos	XPS	[107]
	Oxidation of manganese(II)	XPS	[111]
	Oxidation of bornite	XPS	[101]
	Cobalt on zeolites	XPS	[112]
	Seawater on basaltic glass	XPS	[105]
	Gold on sulfides	XPS	[94]
	Seawater on basaltic glass	XPS	[106]
	Metal ions on clays	XPS/AES	[96]
	Flotation of sulfides	XPS	[113]
	Flotation of sulfides	XPS	[114]
	Hydrogen chloride/water on soils	XPS	[115]
	Chromium complexes on clays	XPS	[98]
	Uranium, thorium on basalt	XPS	[99]
	Flotation of sulfides	XPS	[116]
	Chromium on clays	XPS	[117]
	Mercury on sulfide minerals	XPS	[95]
	Cation exchange on silicates	XPS	[118]
	Copper on sulfide minerals	XPS/AES	[104]
	Cobalt on clays	XPS	[119]

Table 2. (Continued)

Type of Study	System Studied	Technique(s)	Reference
	Chromium on galena	XPS	[103]
	Nickel, copper on clays	XPS	[97]
	Chromium, iron on clays	XPS	[120]
Review	Clay minerals	XPS	[122]
	Clay minerals	XPS	[123]
	Clay minerals and soils	XPS	[124]
	Geochemical processes	XPS	[125]
	Mineral surface chemistry	XPS	[126]

4. *Applications of X–Ray Photoelectron and Combined X–Ray Photoelectron/Auger Spectroscopy.*

4.1. Structure. The first attempts to use x-ray photoelectron to study the surfaces of the aluminosilicates and other similar materials proved to be disappointing. Because the binding energy shifts are small and further confused by sample charging, the results were often conflicting and little progress was made in relating different chemical structures to the x-ray photoelectron spectra. Other reasons for this are that the aluminum and silicon 2p lines are most often broad and weak. Differences in the oxygen 1s spectra, showing hydroxides and oxides (often present for metal oxides), are absent for the aluminosilicates. Differences between the binding energies of silicon 2p and oxygen 1s lines are very similar for many of these compounds. Thus, until recently, many investigators were content to examine the Si/Al ratio of an altered surface as compared with those for the bulk compounds. Over the last few years, significant progress has been made in relating the x-ray photoelectron spectra to the chemical structure of these compounds by carefully examining the Auger parameters, the Auger line shapes, electron-energy loss spectra (plasmon loss), and shape of the valence bands. This is all in addition to carefully measuring the binding energies.

The bulk structure of the aluminosilicates has been extensively studied by many different techniques. The silicate structure can be classified as chains, layers, and networks. Table 3 shows the stoichiometry and formal charge of the various silicate structures. Aluminum can be incorporated into the silicate structure as a cation or as a $[AlO_2]^{-1}$ group tetrahedrally coordinated with the silicate unit. For example, mica, a complex layered structure, contains aluminum bonded both octahedrally as a cation and tetrahedrally with the silicate $Zn[Al_2]\,[Si_3AlO_{10}]\,(OH)_2$. The $[AlO_2]^{-1}$ group can also be bonded to SiO_2 groups in the network systems. This adds a negative charge to the system, typical of the structure for zeolites. If the negative charge is viewed as distributed over the entire group, then the formal charge per silicon atom is proportional to the Al/Si ratio.

Wagner et al. [65] and West and Castle [66] have made useful measurements of the Auger parameter for a number of aluminosilicates and zeolites, producing the Auger parameter plots being shown in Figs. 6 and 7. Good agreement was obtained for both sets of measurements. The silicon Auger parameters for most of the aluminosilicates are similar, but small measurable differences are found. Recall that the Auger parameter can be precisely measured. However, if the Auger parameter is approximately equal for a group of compounds, then the changes in the observed binding energies reflect changes in the electron densities of the initial states. (See Eq. 10). By measuring the Auger parameter, such changes in the initial states may be inferred which cannot be made by just measuring the binding energies alone. By taking the silicates as a group, it is observed that the binding energy of the silicon 2p and oxygen 1s shift is about 0.5–0.6 eV for each unit of formal charge. Note that the difference between the silicon 2p and oxygen 1s is basically constant. The binding energy is highest for

$[SiO_2]^0$ and lowest for $[Si_2O_7]^{-3}$. A similar shift for the zeolites is observed as the negative charge per silicon atom or Al/Si ratio increases. The

Table 3. Summary of Silicate Structures.

Structure	Formal Charge	O/Si Ratio
Isolated silicates	$[SiO_4]^{-4}$	4.0
Dimeric ions	$[Si_2O_7]^{-3}$	3.5
Chains	$[SiO_3]^{-2}$	3.0
Layers	$[SiO_{2.5}]^{-1}$	2.5
Network	$[SiO_2]^0$	2.0

Auger parameter for the aluminum can be roughly divided into two groups. The oxides and octahedrally bonded aluminum cations consist of one group with a slightly higher Auger parameter than for the second group, the zeolites, with aluminum tetrahedrally bonded with the silicate unit. The binding energy of the aluminum 2p line for the zeolites shifts consistently to higher binding energies as the Al/Si ratio decreases, similar to the shift observed for the silicon 2p line. In contrast the silicon oxides possess higher binding energies than the rest of the silicates, while the aluminum oxides possess lower binding energies than the rest of the other aluminosilicates.

Barr and Liska [67] also observed similar shifts in binding energies for aluminum and silicon for the zeolites. They, as have Wagner et al. [65], emphasize that the aluminosilicate species is better viewed as an entire unit with the formal charge distributed among the various atoms. For these compounds the binding energies exhibit shifts from a cluster of atoms rather than from the

separate atoms themselves. As the number of neutral SiO_2 units increases, the negative charge per atom decreases, and the binding energy increases. By taking advantage of such shifts, these authors were able to conclude that especially for the zeolites with Si/Al ratios greater than four, extensive amounts of alumina and sodium aluminate residues were found on the surface in addition to the zeolite structure. When the sodium was removed, mostly alumina was left on the surface. Obviously, it is quite important to characterize the structure of the surface before one can understand the significance of an adsorption experiment.

Barr et al. [68] have also studied the shape of the various valence bands with x-ray photoelectron spectroscopy for a number of the zeolites. They found that the shapes of valence bands for the zeolites differ significantly from those of alumina, silica, or sodium aluminate for Si/Al ratios of one to three. As the amount of aluminum decreases, the valence bands resemble that of silica with small perturbations. Wagner et al. [65] also have compared the shapes of the KVV Auger transitions for oxygen for these compounds. Since the final ionic states have two vacancies in the valence levels, the shape should reflect changes in chemical structure. The shape can be divided into three groups: the aluminas, silicas and zeolites (with Si/Al ratios less than three). Zeolites with large Si/Al ratios are similar to silica. Barr and Lishka [67] also have mentioned that differences in the x-ray photoelectron energy-loss shift ΔE_L exist for the zeolites as compared to alumina and silica.

West and Castle [66] have greatly extended the analysis of the Auger parameter in their study of various aluminosilicates. It has been stated already that changes in the Auger parameter are related to changes in polarizability of the compounds. The index of refraction is also related to the bulk polarizability (P_b) by the Lorentz-Lorentz relationship,

$$\frac{n^2-1}{n^2+2} = \frac{4}{3}\pi\frac{N}{V}P_b \qquad (16)$$

where n is the index of refraction, N Avagadro's number, V is the molar volume. A plot of $(n^2-1)/(n^2+2)$ against the measured Auger parameters for silicon and aluminum demonstrated a good correlation. These authors then suggested that most of the polarizability is accounted for by the oxygen atoms. They also assume that the Auger parameter is directly proportional to the oxygen polarizability P_o.

$$\Delta\alpha = \alpha - \alpha_o = KP_o \qquad (17)$$

The zero point α_o can be estimated from the y-intercept (Auger parameter) or by other means. The K was determined by measuring the Auger parameters for several standards and by using Eq. 16 to calculate P_b. They found that K was dependent upon the coordination of the oxygen: tetrahedrally bonded to silicon, tetrahedrally bonded to aluminum, or octahedrally bonded to aluminum. Excellent correlation was obtained between the oxygen polarizabilities calculated using the Lorentz-Lorentz equation and those derived from the Auger parameters. Many other interesting structural relationship can then be inferred once the polarizabilities have been determined.

For single crystal substrates, photoelectron diffraction has also been used to study changes in the positions of atoms at the surfaces of quite complex minerals. The photoelectron diffraction pattern is obtained by measuring the intensity of a photoelectron line as the angle of the substrate is rotated. The change in intensity as a function of substrate angle can result from a number of different factors. Sample roughness and other instrumental changes can be factored out if the ratio of two lines of approximately the same binding energy are used rather than the absolute values. In this case the changes in the angular distributions will often be

dominated by a diffraction effect. That is, a beam of electrons can act as a wave as it interacts with matter; associated wavelength (λ,in nm) is proportional to its kinetic energy (E_k, in meV)

$$\lambda = \left[\frac{1.5}{E_k}\right]^{1/2} \tag{18}$$

If the electron waves are scattered by an ordered array of atoms, such as in a single crystal, they can be in phase in particular directions in the crystal, or they can be out of phase. If they are in phase, reinforcement will occur, and a strong, scattered beam will be present. If they are out of phase, they will interfere, and a weak beam will be observed. The angular resolution is usually poor in such experiments, so that quantitative information such as d spacings or a partial radial distribution function is not obtained. However, by comparing the angular distributions for a number of pairs of elements, one can say something about the sites they occupy without complicated computations.

Evans et al. [71] have used this technique to investigate the cleavage planes for micas, such as muscovite, lepidolite, phlogopite, and vermiculite. By closely examining the x-ray photoelectron spectral line intensities to obtain atomic ratios and the photoelectron angular intensities to obtain atomic ratios and the photoelectron angular distribution ratios of elemental pairs, they concluded that the structure of the cleavage planes for muscovite and lepidolite were similar to the accepted bulk structure as determined by x-ray diffraction and fluorescence. By comparing the angular distribution ratios for a pair or elements, the equivalency or near-equivalency of atomic position can be inferred. Such analysis indicates that aluminum exists in both tetrahedrally and octahedrally coordinated positions, and potassium and other interlayer cations occupy quite different sites than the silicon. For muscovite, sodium, present in small amounts, was shown to

occupy a slightly different position than the potassium and is not just randomly substituted. The potassium tends to reside in a central position with a coordination number of twelve, while the sodium prefers an off-center position coordinating with six oxygen atoms. For phlogopite and vermiculite, the cleavage planes were found to be rich in aluminum and deficient in magnesium. Interestingly enough, they found that the excess aluminum is tetrahedrally coordinated, giving rise to a deficiency of octahedrally coordinated atoms. Such lattice strains may account for why these planes tend to be preferentially cleaved. For vermiculite the interlayer cations calcium or potassium were exchanged with lead. The potassium and calcium occupy different sites with potassium as anhydrous and calcium as hydrated. The lead after exchange is also hydrated occupying a site similar to the calcium.

Quantitative applications of x-ray photoelectron spectroscopy also have been applied to aluminosilicates. Adams et al. [72] have used relative photoionization cross sections for the 1s, 2s, and 2p subshells obtained from model compound x-ray photoelectron line intensities. The data were then applied to freshly cleaved lepidolite, phlogopite, and muscovite samples to determine atomic ratios. This approach, when compared to more established bulk analytical methods, gave an accuracy of 5%.

Another group of researchers [73] studied the aluminum 2s and 2p photoelectron lines as a function of the aluminum-oxygen bond length. The samples were studied as powders using gold mesh to dissipate charging on the surface. The binding energies of the two main lines showed an increase of approximately 0.5 eV in going from albite and microcline (with Al-O bond distances of 175 pm) to grossularite (195 pm) and α–Al_2O_3 (192 pm). Adams and co-workers [74] also have made a study of the core binding energies of aluminum, along with

those for iron, silicon, magnesium, and oxygen in a series of well-characterized silicate minerals.

X-ray photoelectron spectroscopy has been used to investigate a hollandite ($BaAl_2Ti_6O_{16}$), a zirconolite ($ZrCaTi_2O_7$), and two perovskites [75]. In addition to checking on the agreement of the elemental stoichiometries for the minerals, ion bombardment (sputtering) studies were conducted with respect to both reduction of the titanium and alterations of the titanium 2p photoelectron line shapes. The same studies were conducted with the calcium 2p lines.

4.2. Analysis. X-ray photoelectron and Auger spectroscopy have played an important role in determining the analytical composition of many geologic surfaces. McIntyre et al. [76] have applied the techniques to both surface and bulk studies of trace elements in the coal macerals vitrinite, fusinite, and exinite. In the vitrinite sample, both aluminosilicate and organic phase titanium components were found. The fusinite contained an organofluorine compound and calcium and magnesium dispersed with the fluorine over a large part of the maceral, while the exinite contained lower concentrations of elements than did the other macerals that were studied. Torbanite, gilsonite vitrinite, Kimmeridge kerogen, and brown coal also have been studied by other researchers [77].

One investigation which showed the strength of a combined x-ray photoelectron/Auger approach was one dealing with the surface composition of sediment and soil models [78]. The two model systems studied were ferric oxide, Fe_2O_3, and the clay mineral montmorillonite; the Fe_2O_3 was treated with sodium dihydrogen phosphate, $NaH_2PO_4 \cdot 2H_2O$, in order to approximate the phosphorus: iron atomic ratio of 1:100 found in soil. Figure 8, for example, shows the spectra for montmorillonite samples prepared by two different routes.

The reader should note the difference in the intensity ratio of the Ca 2p/Na KLL lines for the two differently prepared samples. The increase in the calcium intensity in one spectrum was attributed to the formation of a $CaCO_3$–enriched surface during its preparation. The suspected reason for this reaction occurring was the dissolution of carbon dioxide in the water that evaporated from the clay, thus forming a surface-enriched carbonate. This hypothesis was confirmed by preparing the collodial clay sample in an inert, nitrogen atmosphere. The calcium 2p line intensity was greatly diminished; this particular study is a good example of how changing the experimental aspects conform a reaction mechanism for the formation of a surface complex. This same group [79] also has published x-ray photoelectron studies related to the surfaces of sediment reference materials.

4.3. Electronic States. In light of the discussion above regarding the sensitivity of x-ray photoelectron and Auger spectroscopy to the electronic state of elements, it should not be surprising that the two techniques have proved to be powerful tools in expanding the detailed knowledge of geologic materials in this area, particularly in the role of electronic states in bonding. One group of researchers [80] used x-ray photoelectron spectra to determine the Ti^{3+}/Ti^{4+} ratio in synthetic hollandites. The results were compared to those results reported previously for these materials using electron microprobe techniques. X-ray photoelectron spectroscopy has been used by Al-Kadier et al. [81] to study theoretical models for the SiO_4^{4-} species in forsterite, Mg_2SiO_4. This approach, coupled with the analysis of corresponding x-ray emission data for silicon, magnesium, and oxygen, showed the magnesium-oxygen bond. The spatial orientation of the magnesium cations and the SiO_4^{4-} anions appeared to effect sigma-pi mixing of orbitals which could be viewed as either silicon-oxygen bonding or oxygen lone paris.

One area of interest in electronic state studies that has been intensely investigated is that of manganese minerals. Sherman [82] used experimental x-ray photoelectron, x-ray emission, and optical spectra to study manganese oxide minerals. The data were used in conjunction with molecular orbital calculations to examine the clusters MnO_6^{10-}, MnO_6^{9-}, and MnO_6^{8-} corresponding to Mn^{2+}, Mn^{3+}, and Mn^{4+} in octahedral coordination with the O^{2-} oxide anion. The agreement between calculated and experimental spectroscopic transition energies was quite high, indicating that such isolated clusters are very good models for localized electronic structures in manganese oxides. This work also compared the degree of ionicity/covalency in the clusters and the possibility of various spin states for the Mn^{2+}, Mn^{3+}, and Mn^{4+} in manganese oxide minerals.

Evans and Raftery [83] also have used x-ray photoelectron spectroscopy to study the manganese oxides MnO, Mn_3O_4, Mn_2O_3, and MnO_2, along with Norwegian lepidolite. The oxidation state of manganese in the oxides was determined by use of the oxygen 1s and manganese 2p binding energies and the manganese 2p-oxygen 1s binding energy differences. The multiplet splitting of the manganese 3s photoelectron level for the oxides was compared; the multiplet splitting was observed to decrease as the oxidation state of the manganese increased. Two other trends also were identified, both related to the oxidation state of the manganese. First, as the oxidation state increased, the binding energy of the manganese 2p line increased. Second, the manganese 2p-oxygen 1s binding energy separation increased as the oxidation state of the manganese increased. By comparing all of these parameters derived from the model compounds, it was determined that the manganese in the lepidolite samples was present as manganese(II).

Another area in which x-ray-induced photoelectron and Auger spectroscopy have been of tremendous value in increasing the understanding of the electronic state of geologic materials is that of copper minerals. Nakai et al. [84] studied over two dozen copper sulfide minerals to determine the oxidation-state of copper and sulfur. Perry and Taylor [85] were able to distinguish between covellite (CuS) and chalcocite (Cu_2S) by studying their core level binding energy differences, Auger parameters, and lineshape differences. Another study [86] of copper minerals used the extent of the chemical shift in the copper $2p_{3/2}$ binding energy of differentiate the copper(I) and copper(II) oxidation states, along with the absence or presence of satellite structure associated with the main copper $2p_{3/2}$ line.

Other transition element-containing minerals have been studied, including some that have undergone weathering. One group [87] has studied vanadium-bearing aegirines in order to determine the oxidation state of the vanadium, the samples studied included both vanadium aegirites and a barium vanadyl silicate. Iron-containing clay minerals have been studied [88], both in their original state and after they had been reduced and oxidized. Studies [89] have been performed on garnierite which had been formed by the weathering of nickeliferous pyroxenite. Further weathering of the material was shown to induce distinct chemical changes, including the decrease of nickel and silica and an increase in iron(III) and aluminum.

Metal oxide and carbonate minerals have been studied extensively. Taylor and Perry [90] have studied the spectra (Fig. 9) of lead oxide, hydroxide, and carbonate minerals. By exposing clean metallic lead surface to dry oxygen at temperatures below the melting point of lead, the orthorhombic form of PbO (massicot) could be formed as an overlayer mineral. The tetragonal form (litharge),

however, was produced if the same experiment was conducted just at or above the melting point of lead. Air exposure of both the massicot and litharge resulted in carbonate-hydroxide overlayers. Sommer [91] has studied the carbon 1s and oxygen 1s photoelectron lines for a series of carbonate minerals. Allen and co-workers [92] made a comprehensive study of iron oxide and hydroxide minerals, including the effects of multiplet splitting and "shake-up" processes on the main iron $2p_{3/2,1/2}$ photoelectron lines. Chemisorption of water on the minerals was shown to alter the peak lineshapes, and the oxygen 1s peaks attributable to the oxide, hydroxide, and adsorbed water molecules were thoroughly characterized.

4.4. Reaction Chemistry. One of the most important roles of surface techniques in geologic chemistry is that of elucidating the reaction chemistry of species reacting with surfaces. While the number of chemical reaction possibilities is infinite, there are several general areas in which x-ray photoelectron and Auger spectroscopy have been used more than other areas. All of these reaction systems involve geologic substrate/fluid interactions, with the fluid usually being either a liquid such as water or an aqueous solution of an inorganic or organic species. Interactions involving a substrate/gas interface also are possible, but they are less studied; this is possibly due to a perception that such reactions are not as geochemically widespread as are the substrate/liquid reactions. (The reader should be aware of the extreme importance of zeolite/gas interactions in heterogeneous catalysis, for example; this extremely large subfield is beyond the scope of the present work and will not be discussed.) Three of the most common and representative areas of study are metal ion adsorption from aqueous solution, mineral flotation processing, and rock-water type reactions to simulate weathering processes. It is these areas that will be discussed in detail below.

Much work has been reported in the literature related to the adsorption of metal ions on sulfide minerals. Jean and his co-workers [93] have studied the aqueous adsorption of mercury, zinc, cadmium, and lead complexes on sulfide minerals as a function of the solution pH. The adsorption was shown to be heavily dependent on the pH, a factor also directly related to the hydrolysis of the metal ions in solution. Bancroft [94] has reported the low-temperature deposition of gold on pyrite, pyrrhotite, sphalerite, and galena; the deposition mechanism was shown to be the adsorption of the hydrated gold(III) species, followed by its reduction by the sulfide. Brown and his co-workers [95] have published a detailed study of the reaction of elemental mercury and mercury(II) salts with both pyrite and pyrrhotite.

Another area of study that has been extensively reported is that of the adsorption of metal ions on clays, non-sulfide minerals, and rocks. Dillard and co-workers [96] have investigated the surface chemistry of calcined cobalt-kaolinite materials in order to determine the chemical state of the cobalt. Figure 10, for example, shows spectra for a cobalt aluminate standard and a sample of a fired cobalt-clay mixture, the spectra are identical, $CoAl_2O_4$ to be the product of the solid state reaction. This was confirmed by x-ray diffraction. Other studies of metal ion-clay interactions include those of nickel(II) and copper(II) on Kaolinite, chlorite, and illite [97] and the adsorption of chromium(III)-amine complexes on kaolinite, chlorite, and illite [98]. Perry has reported the deposition of uranium and thorium hydrolysis products on the surface of basalt [99].

Surface techniques have also been able to yield extremely important data involving the chemistry of mineral flotation processing. Buckley et al. [100] have studied the surface oxidation of sulfide minerals in flotation. This same group has also studied the oxidation of natural bornite by the atmosphere [101].

Pillai et al. [102] have reported the adsorption of organic xanthates on pyrite, identifying the active collector formed on the surface as being dixanthogen.

Perry and co-workers [103] have reported the reaction of the dichromate ion, $Cr_2O_7^{2-}$, with galena surfaces and shown that both chromium(III) and chromium(VI) species are present on the surface (Fig. 3). This study used model compounds of both chromium(III) and chromium(VI) to determine the surface reaction products, including models such as Cr_2O_3, $Cr(OH)_3$, and $Cr_2O_3 \cdot nH_2O$. The carbon 1s region of the spectrum, in addition to the chromium 2p and oxygen 1s regions, was studied to document the formation of a mixed hydrated oxide/carbonate species as the surface product. Again, as with the case of the manganese oxide/lepidolite study discussed above, the splitting of the 3s photoelectron line was used to study both the model compounds and the reacted galena surface. The spin-orbit splitting differences for chromium(III,VI) that had been reported previously in the literature were used also to verify the two states. The reaction of aqueous copper(II) salts with galena and sphalerite also has been reported [104].

5. *Summary*

The application of x-ray-induced photoelectron and Auger spectroscopies to geologic surface chemistry already has proved to be a powerful tool in gaining a detailed understanding of interfacial reactions. A wide variety of chemical/geochemical systems has been studied, systems that are both naturally-occurring (such as weathering) in the environment and systems created under laboratory conditions. Other studies, such as identifying electronic states of metal ions in minerals, have been invaluable in gaining an understanding of both their solid state chemistry and the reactions they undergo. The expansion of

applications such as these, coupled with yet still to be realized applications, will continue to add to the body of knowledge concerning the field of geologic materials.

6. *Acknowledgments*

One of the authors (DLP) wishes to acknowledge support of his research by the U.S. Department of Energy, Office of Basic Energy Sciences, Division of Engineering and Geosciences, under Contract No. DE-AC03-76SF00098. Additional support has been provided by the Bureau of Mines, U.S. Department of Interior, and the U.S. Nuclear Regulatory Commission.

7. References

[1] Einstein, A. Ann. Phys. (Leipzig) *1905*, 17, 132.

[2] Auger, P. Comp. Rend. *1923*, 177, 169.

[3] Lander, J. J. Phys. Rev. *1953*, 91, 1382.

[4] Siegbahn, K., Ed. "Alpha-, Beta-, and Gamma-Ray Spectroscopy," North Holland Publishing: Amsterdam, 1965.

[5] Harris, L. A. J. Appl. Phys. *1968*, 39, 1419.

[6] Weber, R. E.; Peria, W. T. J. Appl. Phys. *1967*, 38, 4355.

[7] Palmberg, P. W.; Bohn, G. K.; Tracey, J. C. Appl. Phys. Lett. *1969*, 15, 254.

[8] Siegbahn, K.; Nordling, C. N.; Fahlman, A.; Nordberg, R.; Hamrin, K.; Hedman, J.; Johansson, G.; Bergmark, T.; Karlsson, S. E.; Lindren, I.; Lindberg, B., "ESCA, Atomic, Molecular, and Solid State Structure Studied by Means of Electron Spectroscopy," Almqvist and Wiksells: Upsala, 1967.

[9] Siegbahn, K.; Nordling, C.; Johansson, G.; Hedman, J.; Heden, P. F.; Hamrin, K.; Gelius, U.; Bergmark, T.; Werme, L. O.; Manne, R.; Baer, Y., "ESCA Applied to Free Molecules," North-Holland: Amsterdam, 1969.

[10] Brundle, C. R.; Baker, A. D., Eds., "Electron Spectroscopy: Theory, Techniques, and Applications," Academic Press: New York, 1977.

[11] Windawi, H.; Ho, F., Eds., "Applied Electron Spectroscopy for Chemical Analysis," Wiley-Interscience: New York, 1982.

[12] Kane, P. F.; Larrabee, G. B., Eds., "Characterization of Solid Surfaces," Plenum Press: New York, 1974.

[13] Brigg, D.; Seah, M. P., Eds, "Practical Surface Analysis," John Wiley and Sons: New York, 1983.

[14] Carlson, T. A., "Photoelectron and Auger Spectroscopy," Plenum Press: New York, 1975.

[15] Czanderna, A. W., Ed., "Methods of Surface Analysis," Elsevier: New York, 1975.

[16] Thompson, M.; Baker, M. D.; Christie, A.; Tyson, J. F., Eds., "Auger Electron Spectroscopy," Wiley-Interscience: New York, 1985.

[17] Hercules, D. M. Anal. Chem. *1972*, 44, 106R.

[18] Hercules, D. M. Anal. Chem. *1974*, 46, 133R.

[19] Hercules, D. M. Anal. Chem. *1976*, 48, 294R.

[20] Kane, P. F.; Larrabee, G. B. Anal. Chem. *1977*, 49, 221R.

[21] Baker, A. D.; Brisk, M. A.; Liotta, D. C. Anal. Chem. *1978*, 50, 328R.

[22] Kane, P. F.; Larrabee, G. B. Anal. Chem. *1979*, 51, 308R.

[23] Baker, A. D.; Brisk, M. A.; Liotta, D.C. Anal. Chem. *1980*, 52, 161R.

[24] Larrabee, G. B.; Shaffner, T. J. Anal. Chem. *1981*, 53, 163R.

[25] Turner, N. H.; Colton, R. J. Anal. Chem. *1982*, 54, 293R.

[26] Bowling, R. A.; Larrabee, G. B. Anal. Chem. *1983*, 55, 133R.

[27] Turner, N. H.; Dunlap, B. I.; Colton, R. J. Anal. Chem. *1984*, 56, 373R.

[28] Bowling, R. A.; Shaffner, T. J.; Larrabee, G. B. Anal. Chem. *1985*, 57, 130R.

[29] Turner, N. H. Anal. Chem. *1986*, 58, 153R.

[30] McGuire, G. E. Anal. Chem. *1987*, 59, 294R.

[31] Turner, N. H. Anal. Chem. *1988*, 60, 377R.

[32] Riviere, J. C.; In "Solid State Surface Science," Vol. 1; Green, M., Ed.; Dekker: New York, 1969, p. 179.

[33] Wagner, C. D.; Riggs, W. M.; Davis, L. E.; Moulder, J. F.; Muilenberg, G. E. "Handbook of X-Ray Photoelectron Spectroscopy," Perkin-Elmer: Eden Prairie, MN, 1979.

[34] Reference 13, Chapter 5, pp. 181–214.

[35] Wagner, C. D.; Davis, L. E.; Zeller, M. V.; Taylor, J. A.; Raymond, R. H.; Gale, L. H. Surface Interface Analysis *1981*, 3, 211.

[36] Brinen, J. S. In "Electron Spectroscopy," Candano, R.; Verbist, J., Eds.; Elsevier: New York, 1974, p. 377.

[37] Klein, J. C.; Li, C. P.; Hercules, D. M.; Black, J. F. Appl. Spectrosc. *1984*, 38, 729.

[38] Frost, D. C.; Ishitani, A.; McDowell, C. A. Mol. Phys. *1972*, 24, 861.

[39] Sarma, D. D. Indian J. Chem. *1980*, 19, 1046.

[40] Wallbank, B.; Johnson, C. E.; Main, I. G. J. Electron Spectrosc. Relat. Phenom. *1974*, 4, 263.

[41] Yamada, H.; Shriaishi, K.; Watanibe, N. Nippon Kagaku Kaishi *1981*, 8, 1245.

[42] Brundle, C. R.; Chuang, T. J.; Wandelt, K. Surf. Sci. *1977*, 68, 459.

[43] Wagner, C. D.; Biloen, P. Surf. Sci. *1973*, 35, 82.

[44] Wagner, C. D., J. Electron Spectrosc. Relat. Phenom. *1977*, 10, 305.

[45] Wagner, C. D. In "Handbook of X-Ray and Ultraviolet Photoelectron Spectroscopy"; Briggs, D., Ed.; Heyden: London, 1977; Chapter 7.

[46] Frost, D. C.; Ishitani, A.; McDowell, C. A. Mol. Phys. *1972*, 24, 861.

[47] Jolly, W. L. Coord. Chem. Rev. *1974*, 13, 47.

[48] Vernon, G. A.; Stucky, G.; Carlson, T. A. Inorg. Chem. *1976*, 15, 278.

[49] Carver, J. C.; Schweitzer, G. K.; Carlson, T. A. J. Chem. Phys. *1972*, 57, 973.

[50] Aarons, L. J.; Guest, M. F.; Hillier, I. H. J. Chem. Soc., Faraday Trans. *1972*, 68, 1866.

[51] Aberg, T. Phys. Rev. *1967*, 156, 35.

[52] Vernon, G. A.; Stucky, G.; Carlson, T. A. Inorg. Chem. *1976*, 15, 278.

[53] Riviere, J. C. In "Surface Analysis of High Temperature Materials: Chemistry and Topography"; Kemeny, G., Ed.; Elsevier Applied Science Publishers: London, 1984; Chapter 2.

[54] Ritchie, J. M. Phys. Rev. *1957*, 106, 874.

[55] Barrie, A. Chem. Phys. Lett. *1973*, 19, 109.

[56] Kowalczyk, S.P.; Ley, L.; McFeely, F.R.; Pollak, R.A.; Shirley, D.A. Phys. Rev. B. *1974*, 9, 381.

[57] Wagner, C.D. Faraday Discuss. Chem. Soc. *1975*, 60, 291.

[58] Gaarenstroom, S.W.; Winograd, N. J. Chem. Phys. *1977*, 67, 3550.

[59] Wagner, C.D.; Joshi, A. J. Electron Spectrosc. Relat. Phenom. *1988*, 47, 283.

[60] Reference 13, Appendix 4.

[61] Thomas, T.D. J. Electron Spectrosc. Relat. Phenom. *1980*, 20, 117.

[62] Mott, N.F.; Gurney, R.W., "Electronic Processes in Ionic Crystals," Clarendon Press: Oxford, 1948.

[63] Citrin, P.H.; Thomas, T.D. J. Chem. Phys. *1972*, 57, 446.

[64] Kuroda, H.; Ohta, T.; Sato, Y. J. Electron Spectrosc. Relat. Phenom. *1979*, 15, 466.

[65] Wagner, C. D.; Passoja, D. E.; Hillery, H. F.; Kinsky, T. G.; Six, H. A.; Jansen, W. T.; Taylor, J. A. J. Vac. Sci. Technol. *1982*, 21, 944.

[66] West, R. H.; Castle, J. E. Surf. Interface Anal. *1982*, 4, 68.

[67] Barr, T. L.; Lishka, M. A. J. Am. Chem. Soc. *1986*, 108, 3178.

[68] Barr, T. L.; Chen, L. M.; Mohsenian, M.; Lishka, M. A. J. Am. Chem. Soc. *1988*, 110, 7962.

[69] Kubiak, C. J. G.; Aita, C. R.; Tran, N. C.; Barr, T. L. In "Defect Properties and Processing of High-Technology Nonmetallic Materials"; Chen, Y.; Kingery, W. D.; Stokes, R. J., Eds.; Materials Research Society: Pittsburgh, 1984, page 379-386.

[70] Barr, T. L.; Kramer, B.; Shah, I.; Ray, M.; Greene, J. E. In "Thin Films: The Relationship of Structure to Properties"; Aita, C. R.; SreeHarsh, K. S., Eds.; Materials Research Society: Pittsburgh, 1985, page 205-234.

[71] Evans, S.; Adams, J. M.; Thomas, J. M. Philosoph. Trans. Roy. Soc. London *1979*, 292, 563.

[72] Adam, J. M.; Evans, S.; Reid, P.I.; Thomas, J. M.; Walters, M. J. Anal. Chem. *1977*, 49, 2001.

[73] Urch, D. S.; Murphy, S. J. Electron Spectrosc. Relat. Phenom. *1974*, 5, 167.

[74] Adams, I.; Thomas, J. M.; Bancroft, G. M. Earth Planet. Sci. Lett. *1972*, 16, 429.

[75] Myhra, S.; Bishop, H. E.; Riviere, J. C. Surf. Technol. *1983*, 19, 161.

[76] McIntyre, N. S.; Martin, R. R.; Chauvin, W. J.; Winder, C. G.; Brown, J. R.; MacPhee, J. A. Fuel *1985*, 64, 1705.

[77] Clark, D. T.; Wilson, R.; Quirke, J. M. E. Chem. Geol. *1983*, 39, 215.

[78] Soma, M.; Seyama, H. Appl. Surf. Sci. *1981*, 8, 478.

[79] Soma, M.; Seyama, H.; Okamoto, K. Talanta *1985*, 32, 177.

[80] Myhra, S.; White, T. J.; Kesson, S. E.; Riviere, J. C. Am. Mineral. *1988*, 73, 161.

[81] Al-Kadier, M. A.; Tolon, C.; Urch, D. S. J. Chem. Soc. Faraday Trans. II *1984*, 80, 669.

[82] Sherman, D. M. Am. Mineral. *1984*, 69, 788.

[83] Evans, S.; Raftery, E. Clay Miner. *1982*, 17, 477.

[84] Nakai, I.; Sugitani, Y.; Nagashima, K.; Niwa, Y. J. Inorg. Nucl. Chem. *1978*, 40, 789.

[85] Perry, D. L.; Taylor, J. A. J. Mater. Sci. Lett. *1986*, 5, 384.

[86] Nakai, I.; Izawa, M.; Sugitani, J.; Niwa, Y.; Nagashima, K. Mineral. J. *1976*, 8, 135.

[87] Nakai, I.; Ogawa, H.; Sugitani, Y.; Niwa, Y.; Nagashima, K. Mineral. J. *1976*, 8, 129.

[88] Stucky, J. W.; Roth, C. B.; Baitinger, W. E. Clays Clay Miner. *1976*, 24, 289.

[89] Bosio, N. J.; Hurst, V. J.; Smith, R. L. Clays Clay Miner. *1975*, 23, 400.

[90] Taylor, J. A.; Perry, D. L. J. Vac. Sci. Technol. A *1984*, 2, 771.

[91] Sommer, S. Am. Mineral. *1975*, 60, 483.

[92] Allen, G. C.; Curtis, M. T.; Hooper, A. J.; Tucker, P. M. J. Chem. Soc., Dalton Trans. *1974*, 14, 1525.

[93] Jean, G. E.; Bancroft, G. M. Geochim. Cosmochim. Acta *1986*, 50, 1455.

[94] Bancroft, G. M.; Jean, G. Nature (London) *1982*, 298, 730.

[95] Brown, J. R.; Bancroft, G. M.; Fyfe, W. S.; McLean, R. A. N. Environ. Sci. Technol. *1979*, 13, 1142.

[96] Dillard, J. G.; Schenck, C. V.; Koppelman, M. H. Clays Clay Miner. *1983*, 31, 69.

[97] Koppelman, M. H.; Dillard, J. G. Clays Clay Min. *1977*, 25, 457.

[98] Koppelman, M. H.; Dillard, J. G. Clay Clay Min. *1980*, 28, 211.

[99] Perry, D. L. In "NRC Nuclear Waste Geochemistry '83", Alexander, D. H.; Birchard, G. F., Eds.; U.S. Nuclear Regulatory Commission Report No. NUREG/CP-0052, Washington, D.C., 1983; Chapter 2.2.

[100] Buckley, A. N.; Hamilton, I. C.; Woods, R. Dev. Miner. Process. *1985*, 6[Flotation Sulphide Miner.], 41.

[101] Buckley, A. N.; Woods, R. Aust. J. Chem. *1983*, 36, 1793.

[102] Pillai, K. C.; Young, V. Y.; Bockris, J. O'M. J. Colloid Interface Sci. *1985*, 103, 145.

[103] Perry, D. L.; Tsao, L.; Taylor, J. A. Inorg. Chim. Acta *1984*, 85, L57.

[104] Perry, D. L.; Tsao, L.; Taylor, J. A. Proc. Electrochem. Soc. *1984*, 84-10[Proc. Int. Symp. Electrochem. Miner. Met. Process., 1984], 169.

[105] Crovisier, J. L.; Thomassin, J. H.; Juteau, T.; Eberhart, J. P.; Touray, J. C.; Baillif, P. Geochim. Cosmochim. Acta *1983*, 47, 377.

[106] Crovisier, J. L.; Eberhart, J. P.; Thomassin, J. H.; Juteau, T.; Touray, J. C.; Ehret, G. C. R. Seances Acad. Sci., Ser. 2 *1982*, 294, 989.

[107] Thomassin, J. H.; Touray, J. C.; Baillif, P.; Jaurand, M. C.; Magne, L.; Goni, J. IARC Sci. Publ. *1980*, 30[Biol. Eff. Miner. Fibres, vl], 105.

[108] Brown, J. R.; Fyfe, W. S.; Bancroft, G. M. Appl. Surf. Sci. *1981*, 7, 419.

[109] Goelander, C. G.; Eriksson, J. C. J. Colloid Interface Sci. *1987*, 119, 38.

[110] Claesson, P. M.; Herder, P.; Stenius, P.; Eriksson, J. C.; Pashley, R. M. J. Colloid Interface Sci. *1986*, 109, 31.

[111] Murray, J. W.; Dillard, J. G.; Giovanoli, R.; Moers, H.; Stumm, W. Geochim. Cosmochim. Acta *1985*, 49, 463.

[112] Lunsford, J. H.; Hutta, P. J.; Lin, M. J.; Windhorst, K. A. Inorg. Chem. *1978*, 17, 606.

[113] Predali, J. J.; Brion, D.; Hayer, J.; Pelletier, B. Dev. Miner. Process. *1981*, 2[Miner. Process., Part A, Volume Date 1979], 134.

[114] Nefedov, V. I.; Salyn, Y. V.; Solozhenkin, P. M.; Pulatov, G. Y. Surf. Interface Anal. *1980*, 2, 170.

[115] Kang, Y.; Pellett, G. L.; Skiles, J. A. Wightman, J. P. J. Colloid Interface Sci. *1980*, 75, 313.

[116] Predali, J. J.; Brion, D.; Hayer, J.; Pelletier, B. 13th Int. Mineral. Process. Congr. *1979*, 1, 55.

[117] Koppelman, M. H.; Emerson, A. B.; Dillard, J. G. Clays Clay Miner. *1980*, 28, 119.

[118] Adams, J. M.; Evans, S. Clays Clay Miner. *1979*, 27, 248.

[119] Koppelman, M. H.; Dillard, J. G. J. Colloid Interface Sci. 1978, 66, 345.

[120] Koppelman, M. H.; Dillard, J. G. ACS Symp. Ser., 1975, 18[Mar. Chem. Coastal Environ.], 186.

[121] Landis, W. J.; Martin, J. R. J. Vac. Sci. Technol., A. *1984*, 2, 1108.

[122] Canesson, P. Dev. Sedimentol. 1982, 34[Adv. Tech. Clay Miner. Anal.], 211.

[123] Koppelman, M. H. NATO Adv. Study Inst. Ser., Ser. C 1980, 63[Adv. Chem. Methods Soil Clay Miner. Res.], 205.

[124] Defosse, C.; Rouxhet, P. G. NATO Adv. Study Inst. Ser., Ser. C 1980, 63[Adv. Chem. Methods Soil Clay Miner. Res.], 169.

[125] Bancroft, G. M.; Brown, J. R.; Fyfe, W. S. Chem. Geol. *1979*, 25, 227.

[126] Koppelman, M. H.; Dillard, J. G. Dev. Sedimentol. *1979*, 27[Int. Clay Conf. Proc., 6th, 1978], 153.

FigureCaptions

Figure 1. Schematic representation for the x-ray photoelectron and Auger electron formation processes.

Figure 2. The x-ray photoelectron survey spectrum of galena, PbS, reacted with aqueous sodium dichromate, $Na_2Cr_2O_7$.

Figure 3. The high resolution chromium $2p_{3/2,1/2}$ x-ray photoelectron spectrum of galena, PbS, reacted with aqueous sodium dichromate, $Na_2Cr_2O_7$. [Adapted from Ref. 103]

Figure 4. High resolution x-ray photoelectron spectra of the aluminum 2s region of a clean, evaporated aluminum film (lower) and the same film after exposure to oxygen at atmospheric pressure for thirty minutes. [Adapted from Ref. 55]

Figure 5. X-ray photoelectron spectrum of sodium hydrogen phosphate, Na_2HPO_4,showing the Auger parameter. [Adapted from Ref. 59]

Figure 6. Aluminum chemical state plot for aluminum-oxygen compounds. [Reprinted from Ref. 65 with permission]

Figure 7. Silicon chemical state plot for silicon-oxygen compounds. [Reprinted from Ref. 65 with permission]

Figure 8. Calcium 2p and carbon 1s region of the x-ray photoelectron spectrum of powdered montmorillonite as received (top) and as a dried, aqueous colloidal suspension (bottom). [Adapted from Ref. 78]

Figure 9. Oxygen KVV and 1s lines for a) PbO(massicot), b) same PbO sample heated *in situ* in O_2, c) clean, metallic lead exposed to O_2 at 150 °C, d) PbO_2 (plattnerite), e) same PbO_2 heated to 320 °C *in vacuo*, f) Pb_3O_4 (minimum), and g) 2 $PbCO_3 \cdot Pb(OH)_2$ (hydrocerussite). [Reprinted from Ref. 90 with permission]

Figure 10. High resolution x-ray photoelectron cobalt $2p_{3/2,1/2}$ spectra for $CoAl_2O_4$ (top) and an air-calcined mixture of $Co(NH_3)_6Cl_3$ and kaolinite hydrite PX (bottom). [Adapted from Ref. 96]

Figure 1.

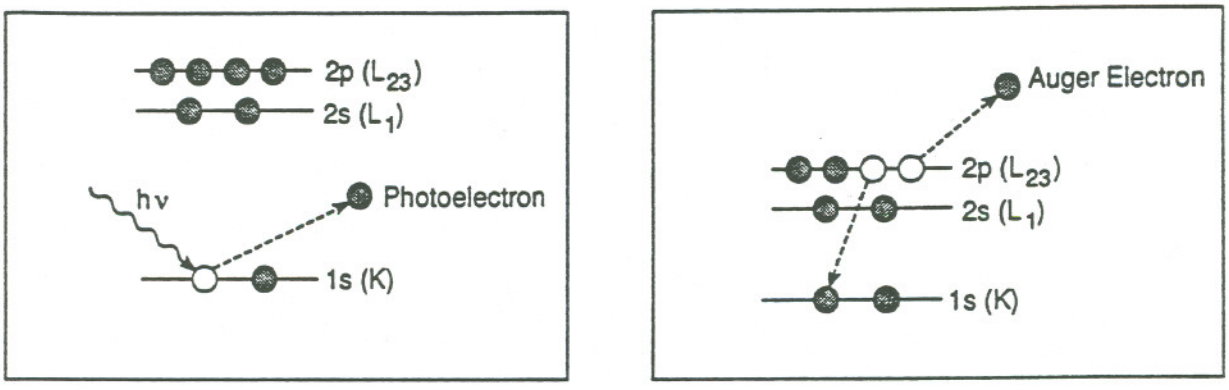

XBL 8812-10560

Figure 2.

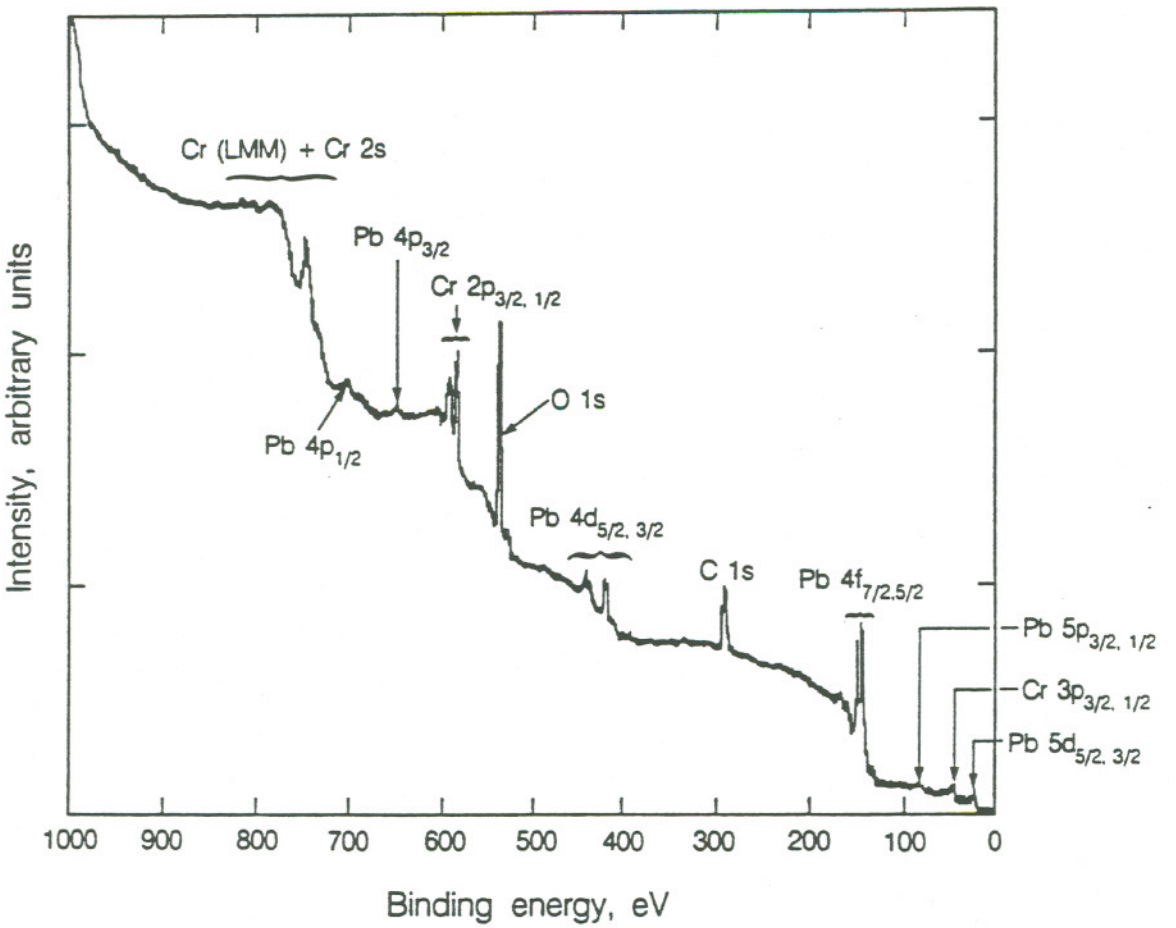

XBL 8812-10614

Figure 3.

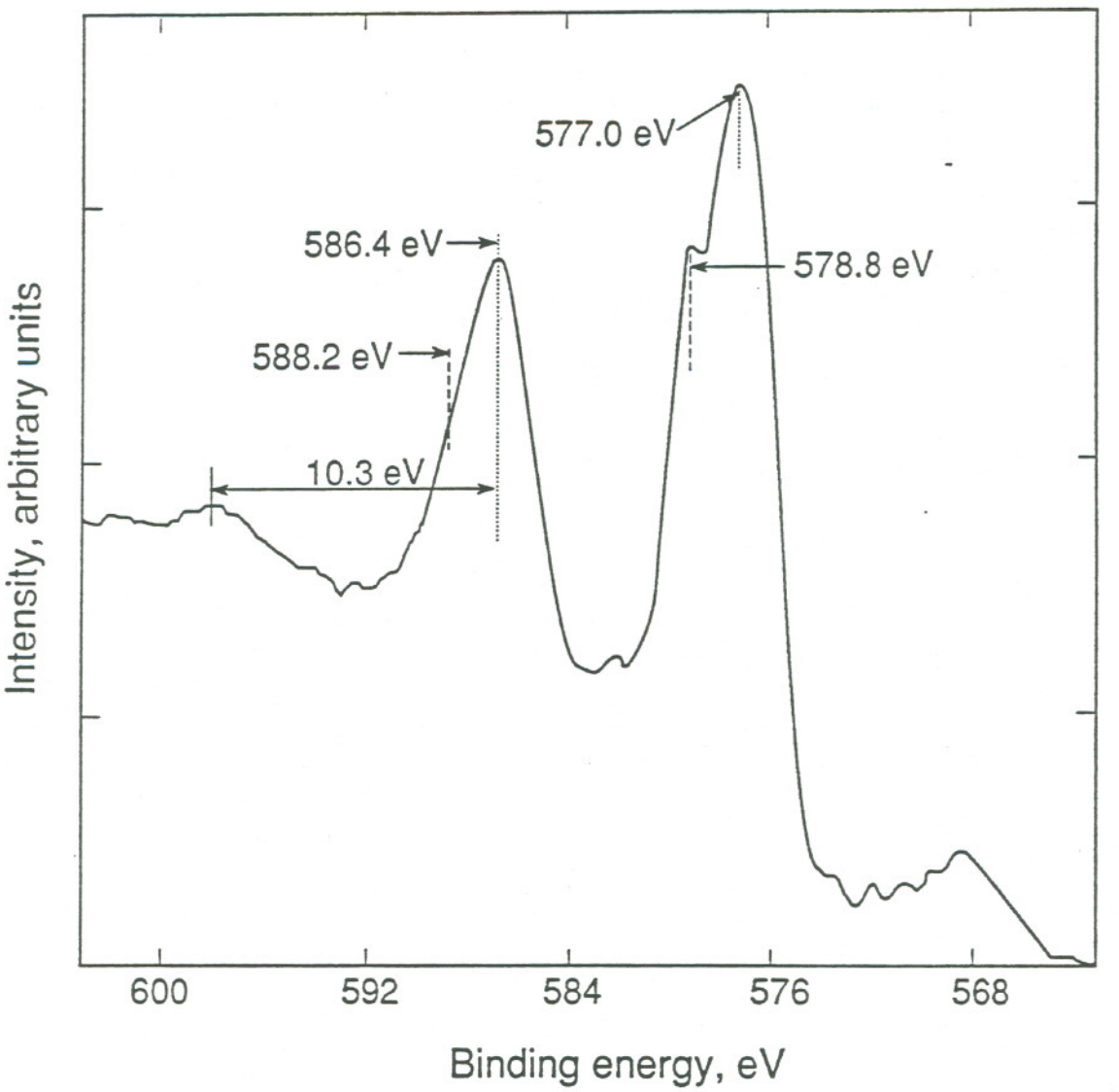

XBL 8812-10613

Figure 4.

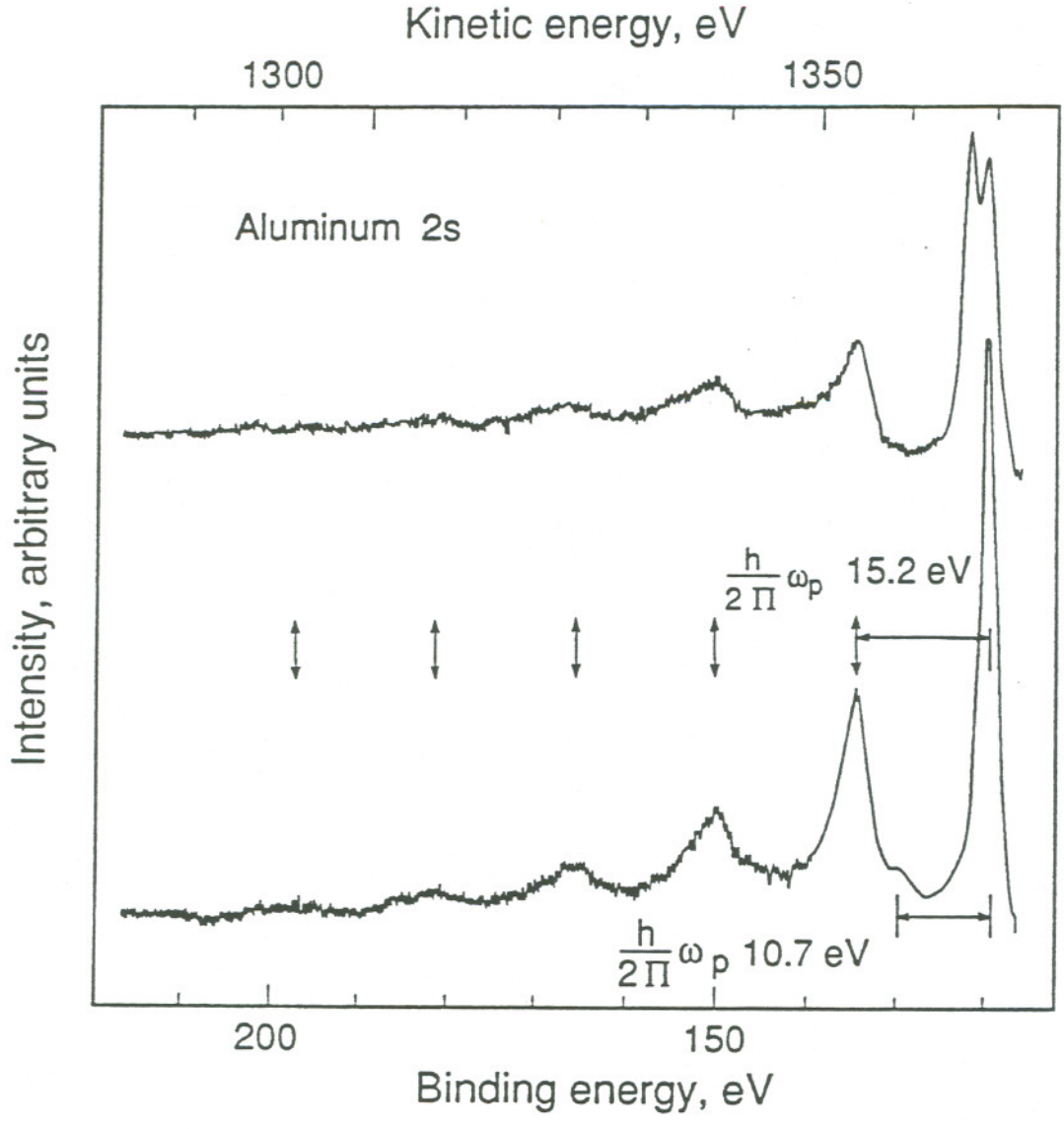

XBL 895-7574

Figure 5.

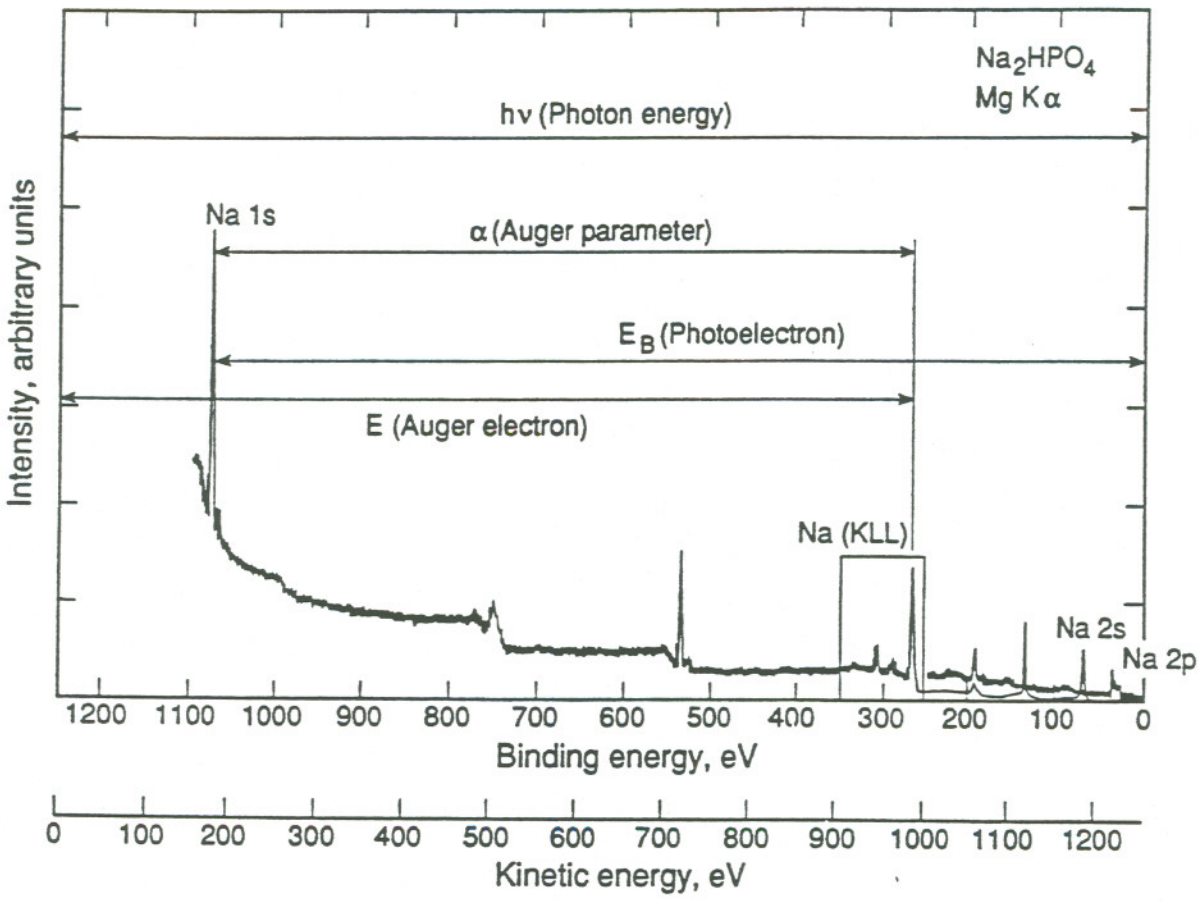

XBL 896-7635

Figure 6.

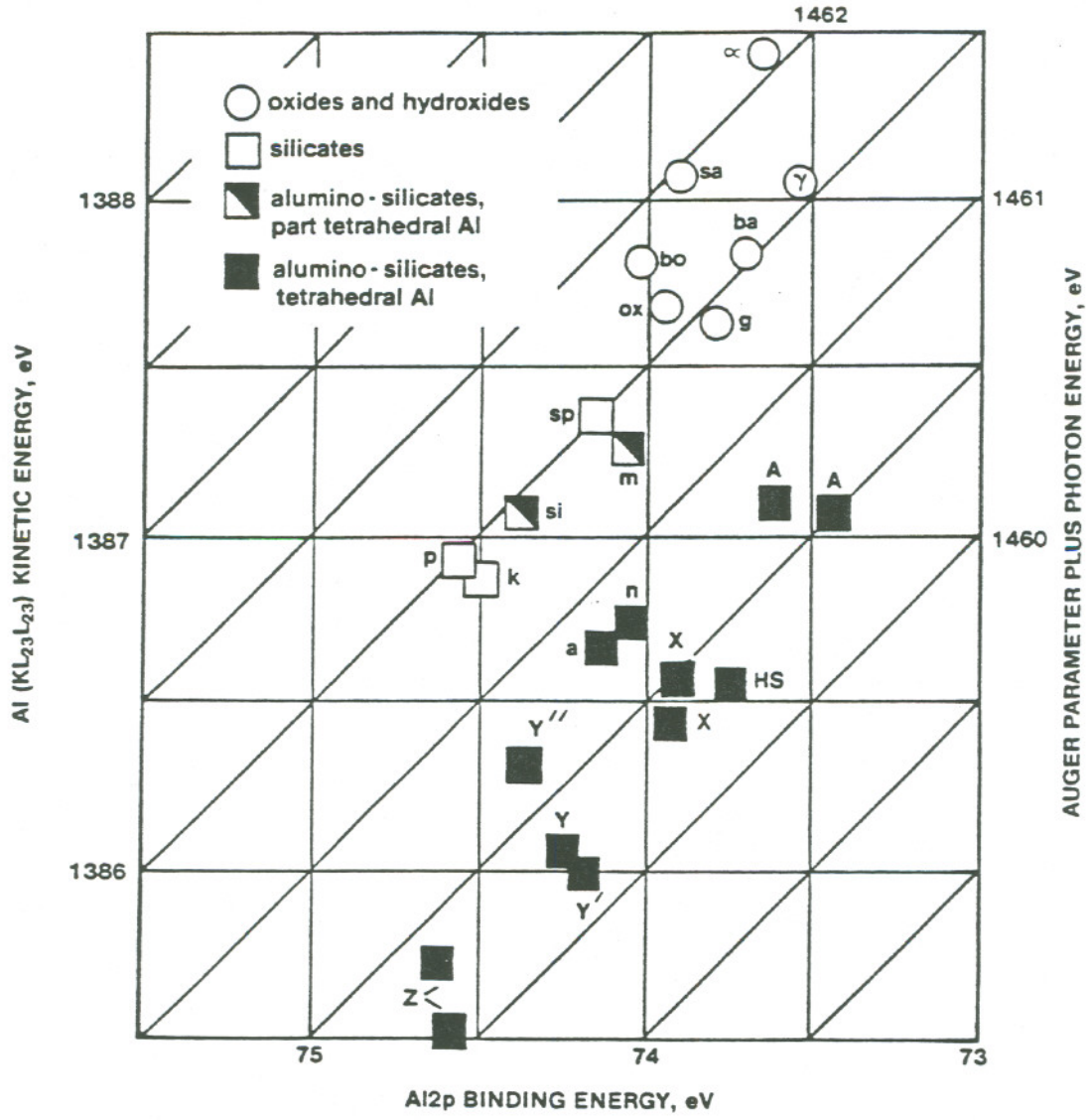

sa	sapphire	si	sillimanite
∝	∝ - alumina	m	muscovite mica
γ	γ - alumina	a	albite
ox	oxidized aluminum	n	natrolite
bo	boehmite	A	molecular sieve type A
ba	bayerite	X	molecular sieve type X
gi	gibbsite	Y	molecular sieve type Y
sp	spodumene	Y′	molecular sieve type Y
p	pyrophyllite	Y″	molecular sieve type Y
k	kaolinite	Z	H Zeolon
		HS	hydroxysodalite

XBL 896-2279

Figure 7.

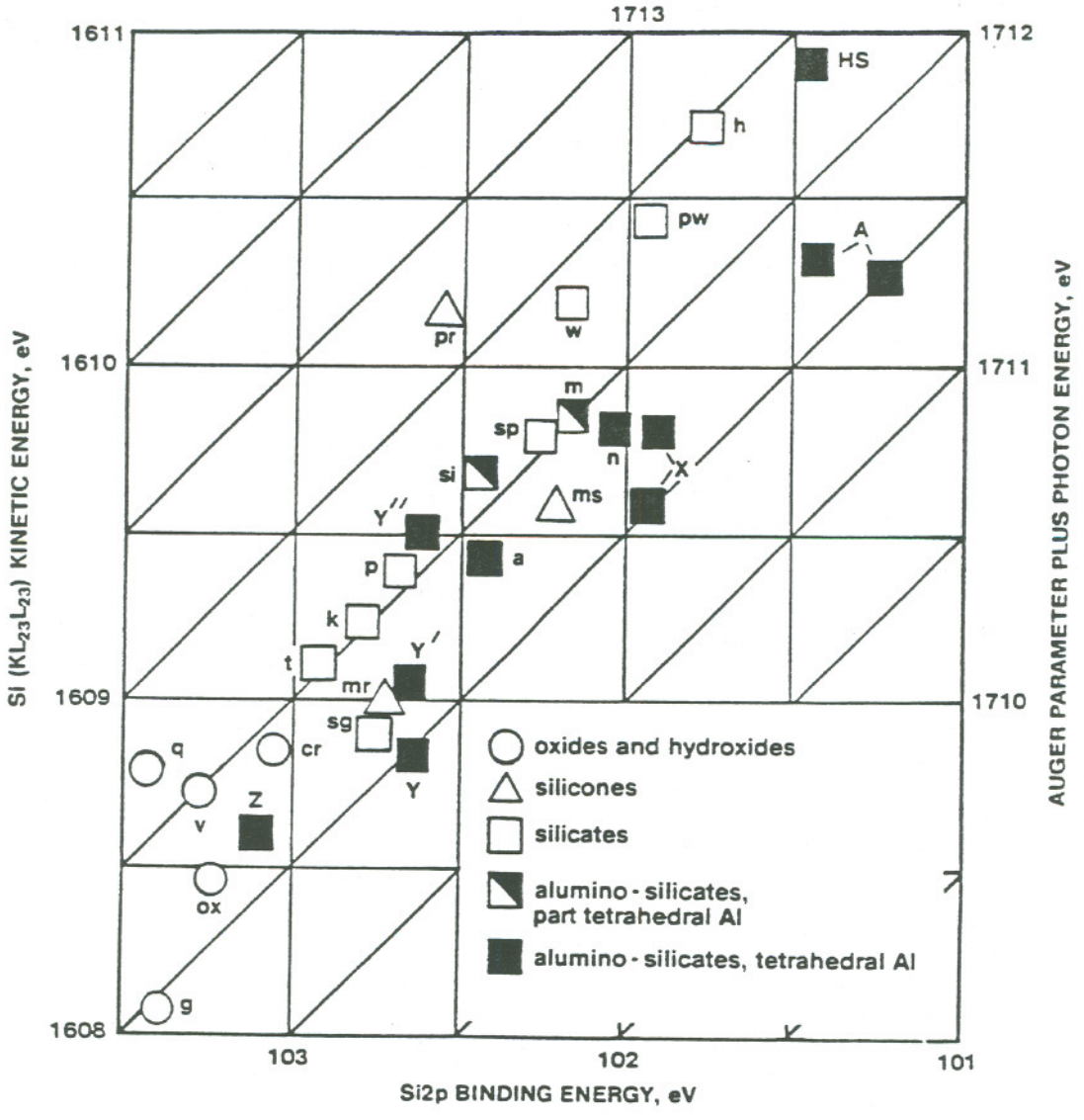

ms	dimethylsilicone polymer
mr	methylsilicone resin
pr	phenylsilicone resin
q	α – quartz
v	vycor
cr	α - cristobalite
g	silica gel
ox	oxidized silicon
w	wollastonite
h	hemimorphite
k	kaolinite
p	pyrophyllite
sg	soda glass
t	talc
pw	pseudowollastonite
sp	spodumene
si	sillimanite
m	muscovite mica
n	natrolite
A	molecular sieve type A
X	molecular sieve type X
Y	molecular sieve type Y
Y′	molecular sieve type Y
Y″	molecular sieve type Y
Z	H Zeolon
HS	hydroxysodalite
a	albite

XBL 896-2280

Figure 8.

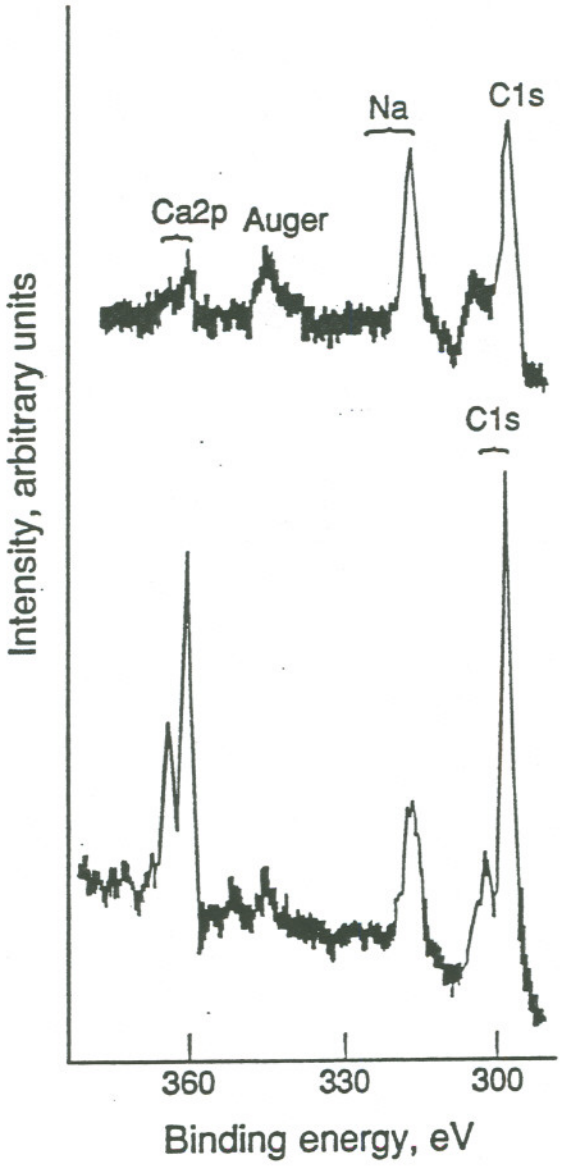

XBL 895-7577

Figure 9.

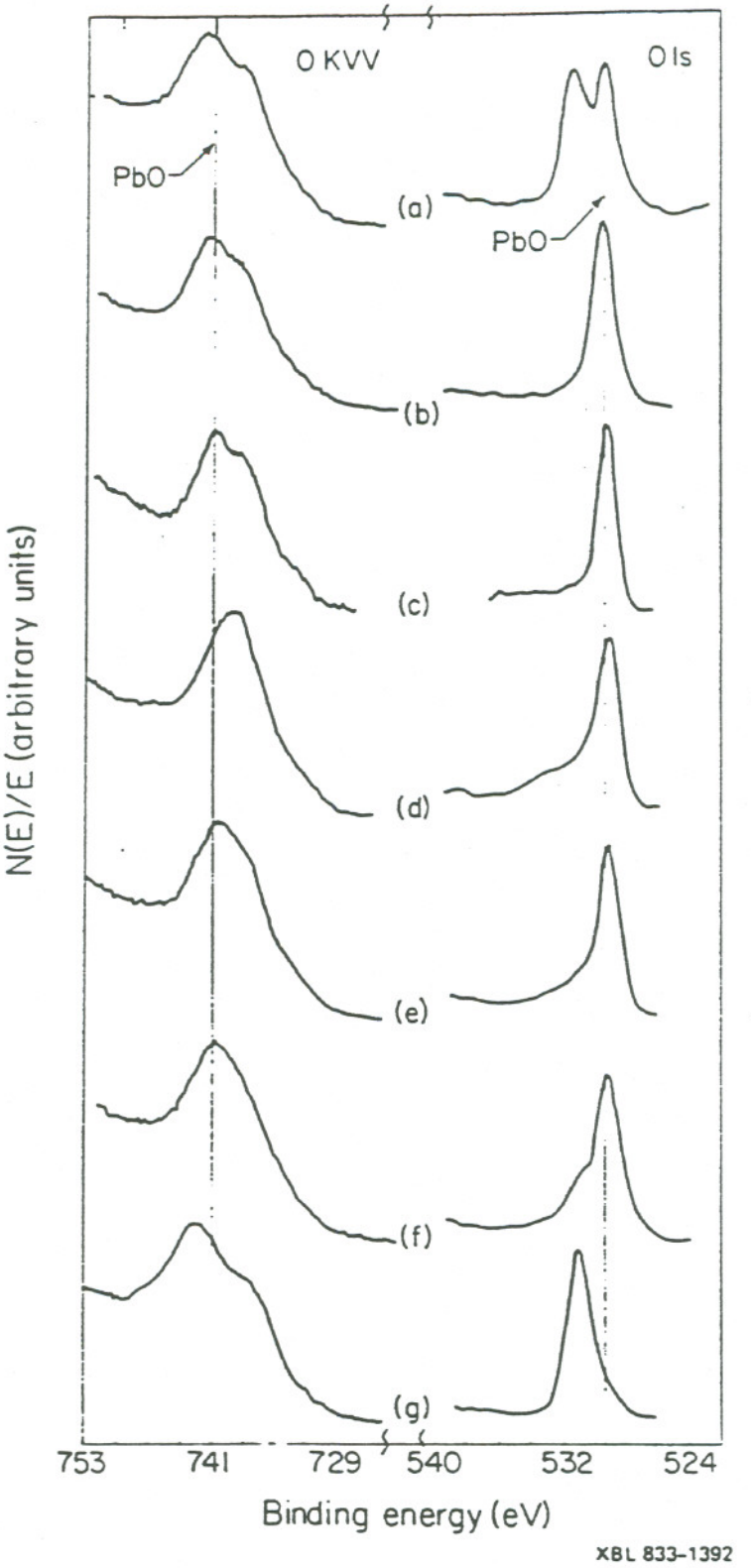
O KVV
O 1s
PbO
PbO
(a)
(b)
(c)
(d)
(e)
(f)
(g)
N(E)/E (arbitrary units)
753
741
729
540
532
524
Binding energy (eV)
XBL 833-1392

Figure 10.

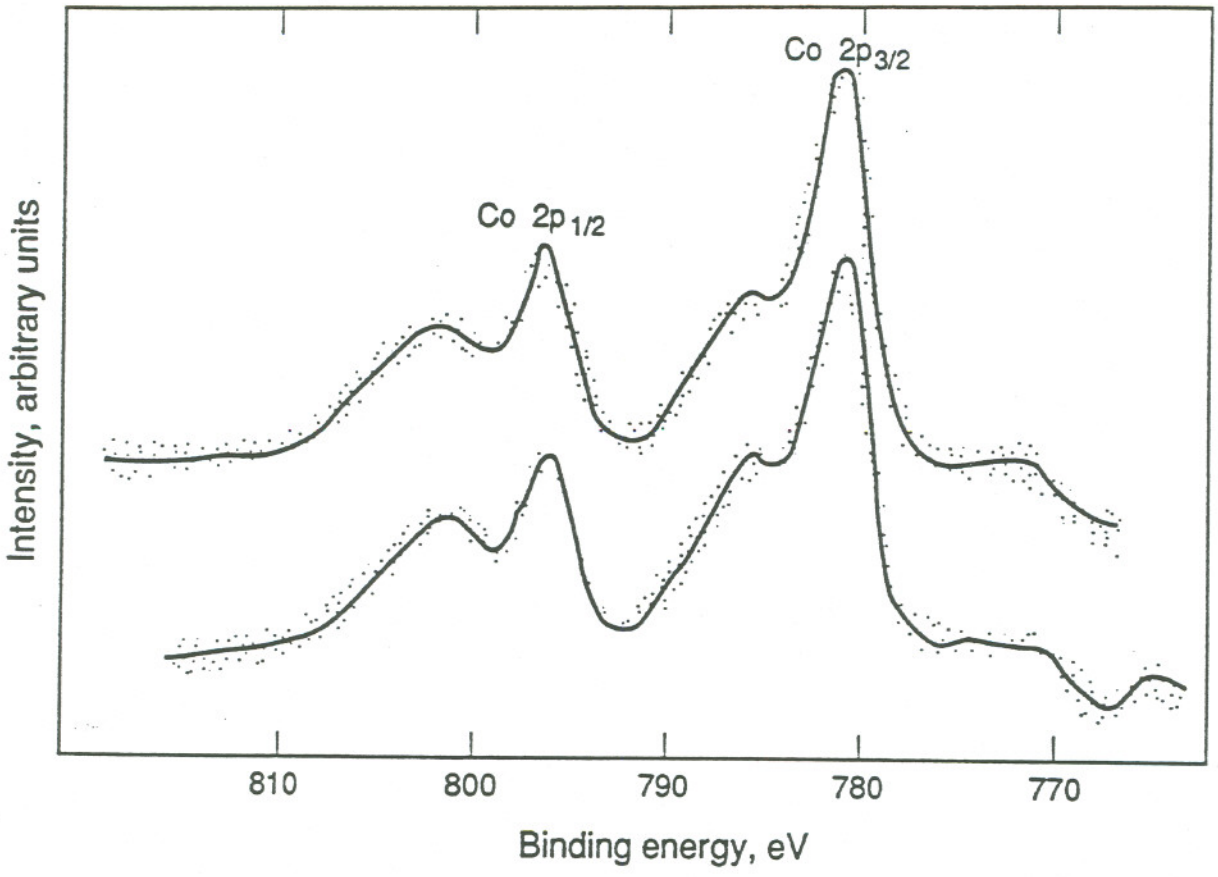

XBL 895-7576